

Insights from a New High-Resolution Drought Atlas for the Caribbean Spanning 1950–2016

DIMITRIS HERRERA AND TOBY AULT

Department of Earth and Atmospheric Sciences, Cornell University, Ithaca, New York

(Manuscript received 23 November 2016, in final form 14 June 2017)


ABSTRACT

Climate change is expected to increase the severity and frequency of drought in the Caribbean. Understanding drought variability and its trends is therefore critical for improving resiliency and adaptation capacity of this region, as well as for assessing the dynamics and predictability of regional hydroclimate across spatial and temporal scales. This work introduces a first of its kind high-resolution drought dataset for the Caribbean region from 1950 to 2016, using monthly estimates of the “self-calibrating” Palmer drought severity index (scPDSI), with the physically based Penman–Monteith approximation for the potential evapotranspiration. Statistically downscaled data products, including reanalysis, are employed to establish an historical baseline for characterizing drought from 1950 to the near present. Since 1950, the Caribbean has been affected by severe droughts in 1974–77, 1997/98, 2009/10, and 2013–16. Results indicate that the 2013–16 drought is the most severe event during the time interval analyzed in this work, which agrees with qualitative reports of many meteorological institutions across the Caribbean. Linear trends in the scPDSI show a significant drying in the study area, averaging an scPDSI change of $-0.09 \text{ decade}^{-1}$ ($p < 0.05$). However, this trend is not homogenous, and significant trends toward wetter conditions in portions of the study area were observed. Results further indicate a strong influence of both tropical Pacific and North Atlantic oceans in modulating drought variability across the study domain. Finally, this effort is the first step in building high-resolution drought products for the Caribbean to be updated regularly, with the purpose of drought monitoring and eventually seasonal drought prediction.

1. Introduction

Droughts are among the deadliest and costliest natural phenomena, leading to food shortages and annual losses of billions of dollars worldwide (e.g., Wilhite et al. 2007; Howitt et al. 2014). Although droughts do not unfold as rapidly as other meteorological hazards (e.g., hurricanes or floods), their duration can put food security, water storage, and even energy production at risk. A drought is usually characterized by below-normal precipitation, and often associated with above-normal temperatures that may span from several months to years and, in some cases, decades (Dai 2011; Cook et al. 2016). From observations and model simulations, previous studies have shown an increase of the global

drought area since 1950 (Dai et al. 2004; Dai 2011, 2013; Dai and Zhao 2017; van der Schrier et al. 2013; Cook et al. 2015). These findings further correspond to increasing global temperatures and hence evaporative demand, which in turn has been identified as a crucial driver in the observed trend (Dai 2013; Dai and Zhao 2017; van der Schrier et al. 2013; Cook et al. 2015; Zhao and Dai 2015). Furthermore, projections from phases 3 and 5 of the Coupled Model Intercomparison Project (CMIP3 and CMIP5) have suggested a substantial increase in global aridity by the end of the twenty-first century as a consequence of rising concentrations of greenhouse gases (Dai 2013; IPCC 2014; Ault et al. 2014; Cook et al. 2015; Zhao and Dai 2015). Model simulations also indicate that the greatest decline in precipitation will occur in certain areas of the tropics and subtropics, where rainfall could be reduced by as much as 50% on average in regions like the Caribbean and Central America (IPCC 2014; Zhao and Dai 2015). In addition to these rainfall shortages, higher future temperatures could lead to even more severe droughts due

 Denotes content that is immediately available upon publication as open access.

Corresponding author: Dimitris Herrera, dah386@cornell.edu

DOI: 10.1175/JCLI-D-16-0838.1

© 2017 American Meteorological Society. For information regarding reuse of this content and general copyright information, consult the [AMS Copyright Policy](#) (www.ametsoc.org/PUBSReuseLicenses).

to an increased atmospheric demand of moisture (Dai 2013; IPCC 2014; Cook et al. 2014, 2015; Zhao and Dai 2015). Consequently, this would drive or worsen drought risk even if precipitation does not change appreciably from historical averages (Cook et al. 2015; Ault et al. 2016).

Although many regional subtropical drying trends are robust across observational and model studies (IPCC 2014; Ault et al. 2014; Cook et al. 2015; Zhao and Dai 2015), large uncertainties in this picture originate from differences in data and models used for assessing drought. For example, Dai and Zhao (2017) calculated the Palmer drought severity index (PDSI)—a widely used indicator of agricultural drought—using different underlying climate data products. They found that historical trends and variances of the PDSI are sensitive to differences between observational data products (especially precipitation, net radiation, and wind speed) and the calibration period used to normalize the index, although the latter has a smaller contribution than the underlying climate data. In terms of future projections of drought, both CMIP3 and CMIP5 are consistent in showing increased global aridity in the twenty-first century. Major differences among models are mostly due to discrepancies in projected precipitation (Zhao and Dai 2015, 2017). However, uncertainties in future projections of drought still persist on simulated regional trends and variances, which could be due to the dominant influence of the natural internal variability of drought at regional scales (Dai 2013; Zhao and Dai 2015, 2017).

The Caribbean region is vulnerable to climate change as a result of more severe and widespread droughts observed and projected at the end of the twenty-first century (IPCC 2014; Stephenson et al. 2014, 2016). The greatest decline in rainfall projected for the Caribbean might occur during boreal summer (June–August; Rauscher et al. 2008; Campbell et al. 2011; Karmalkar et al. 2011; IPCC 2014), a critical season for capturing and storing water in many countries of the region. In addition, the inherent insular nature of the Caribbean islands makes them especially vulnerable to drought because water cannot be collected, moved, or stored on large spatial scales (as it can be in the U.S. Southwest). Recent studies have also indicated that many of the small islands in the Caribbean Sea will face unprecedented freshwater and groundwater stresses because of climate change (e.g., Holding et al. 2016; Karnauskas et al. 2016). The region is made even more vulnerable by its dense population and limited economic growth, most of which depends on tourism and a poorly developed agricultural sector (Sahay 2005; Martin and Schumacher 2011; IPCC 2014).

Instrumental and historical records document the occurrence of multiyear droughts in the Caribbean and Central America during the last 60 years (e.g., Larsen 2000; Méndez and Magaña 2010; Peters 2015; Blunden and Arndt 2016). These events have caused water shortages in agriculture, energy generation, and municipal usage, affecting the economies of many countries in the region (Larsen 2000; Peters 2015; OCHA 2015; FAO 2016). Some of those dry intervals have been linked to the warm phase of El Niño–Southern Oscillation (ENSO; Peters 2015; Blunden and Arndt 2016), including the 1997/98, 2009/10, and 2013–16 droughts. The recent drought between 2013 and 2016 has been referred to as the most severe event in over 50–100 years in many countries of the Caribbean and Central America by some of their public institutions (e.g., DRNA 2016; IMN 2016), although this claim lacks firm quantitative backing because of the paucity of hydroclimatic data in the region. While the effects of this event have not yet been fully quantified, agricultural losses of over \$200 million have been estimated in El Salvador and Guatemala (OCHA 2015; FAO 2016). For reference, the gross domestic product of these two countries was \$25.85 and \$63.79 billion, respectively, in 2015 according to the World Bank.

Although the Caribbean is likely to be affected by drought and freshwater stress in the future, there is currently no single study characterizing historical droughts and their trends at a spatial resolution appropriate for the topography of the region. A few studies have used data from weather stations, but they do not fully cover the entire region (e.g., Larsen 2000; Giannini et al. 2000, 2001a,b; Taylor et al. 2002; Jury et al. 2007; Peters 2015; Blunden and Arndt 2016). Regional and global station datasets, such as the National Oceanic and Atmospheric Administration (NOAA) Global Historical Climatology Network (GHCN), are missing a considerable amount of data in many sites in the Caribbean region and Central America, and many of the data that do exist are of inconsistent quality (Blunden and Arndt 2016). Furthermore, existing gridded drought products (e.g., Dai et al. 2004; Dai 2011; Vicente-Serrano et al. 2010; Sheffield et al. 2012; van der Schrier et al. 2013) are generated at spatial scales of 50–100 km. At these scales, spatial variations in drought associated to the complex topography of many islands in the Caribbean Sea cannot be resolved. For example, a single grid cell of 0.5°, the highest resolution drought datasets currently available (Vicente-Serrano et al. 2010; van der Schrier et al. 2013) covers more than twice the area of Martinique (~1200 km²). Therefore, products like this

TABLE 1. Monthly climate datasets used in this work.

| Variable | Dataset | Native resolution | Period used | Reference |
|-------------------------------------|-------------------------|-------------------|----------------------------|---------------------------------------|
| Precipitation | GPCC V7 | 1° | 1949–2016 | Schneider et al. (2015a,b) |
| | CHIRPS | 0.05° | 1981–2016 | Funk et al. (2015) |
| | WorldClim (climatology) | ~1 km | 1950–2000 | Hijmans et al. (2005) |
| | CHELSA (climatology) | ~1 km | 1979–2013 | Karger et al. (2016) |
| Temperature | BEST | 1° | 1949–2016 | Rohde et al. (2013) |
| | NCEP–NCAR reanalysis | 2.5° | 1949–2016 | Kalnay et al. (1996) |
| | WorldClim (climatology) | ~1 km | 1950–2000 | Hijmans et al. (2005) |
| Cloud cover | NCEP–NCAR reanalysis | ~2° | 1949–2016 | Kalnay et al. (1996) |
| Wind speed | NCEP–NCAR reanalysis | 2.5° | 1981–2010 (climatology) | Kalnay et al. (1996) |
| Elevation | WorldClim | ~1 km | — | Hijmans et al. (2005) |
| Available water holding capacity | IGBP-DIS | 0.08° | — | Global Soil Data Task Group (2000) |

one are not suitable for assessing the effects of local topography on enhancing or diminishing drought in the Caribbean or for evaluating how topography might influence the interannual variability and decadal trends of drought in the region. These products were also not designed to be regularly updated at monthly time scales while still providing an internally consistent picture of historical variations.

Given the limitations of existing products for characterizing and monitoring drought at small spatial scales in the Caribbean and Central America, here we introduce a high-resolution gridded drought dataset based on the “self-calibrating” PDSI (scPDSI; Wells et al. 2004) that spans 1950–2016. Our results yield an atlas that is relevant to stakeholders and researchers alike. It can further be updated on a monthly basis for ongoing drought monitoring and relief efforts. (Our atlas is available online at <http://ecrl.eas.cornell.edu/products/caribbean-drought/index.html>.)

2. Data and methods

a. Data

The climate data products used in this work are listed in Table 1. To calculate potential evapotranspiration (PET), we used statistically downscaled National Centers for Environmental Prediction (NCEP)–National Center for Atmospheric Research (NCAR) reanalysis data (Kalnay et al. 1996) of monthly averages of temperature (T_{\max} , T_{mean} , and T_{\min}), cloud cover (to derive the net radiation), and wind speed that have native resolutions of approximately 1.8° and 2.5° in latitude and longitude (~200 and ~280 km, respectively). To assess the consistency of downscaled reanalysis temperature products, we also used gridded monthly temperature means from the 1° Berkeley Earth

Surface Temperature (BEST) dataset (Mueller et al. 2013; Rohde et al. 2013). The BEST dataset incorporates approximately 400 land-weather stations in our study domain (defined as the region 6°–30°N, 90°–60°W; Fig. 1), including data from the GHCN and other global and regional climate data networks (Rohde et al. 2013). As compared to similar products, the number of records used by BEST is substantially higher. For example, the University of East Anglia Climatic Research Unit (CRU) Time Series, version 3.24 (TS3.24), dataset (Harris et al. 2014) currently uses less than a hundred temperature stations in the Caribbean and Central America. BEST further differs from other global temperature datasets in the manner of treating temperature data, in which stations with discontinuities (e.g., missing data) are split and treated as different series, rather than undergoing a homogenization process (Mueller et al. 2013; Rohde et al. 2013). Split stations are then weighted based on their accuracy, as evaluated from nearby stations using a kriging approach (Rohde et al. 2013). The details of the method implemented to construct this dataset are available in Rohde et al. (2013). The BEST dataset is further updated on a regular basis, which is advantageous for drought monitoring.

Gridded monthly totals of precipitation were obtained from the Global Precipitation Climatology Centre (GPCC), version 7 (V7), land surface dataset (Schneider et al. 2015a), which is based on 75 000 quality-controlled rain gauges worldwide, including approximately 400 in the Caribbean and Central America. We used the GPCC V7 “combined product” (<http://www.esrl.noaa.gov/psd/data/gridded/data.gpcc.html>), with a native resolution of 1° (Schneider et al. 2015b). This version incorporates the full dataset from 1901 to 2014 with a monitoring product spanning from 2014 to the near present. Although various gridded precipitation products are currently available, we

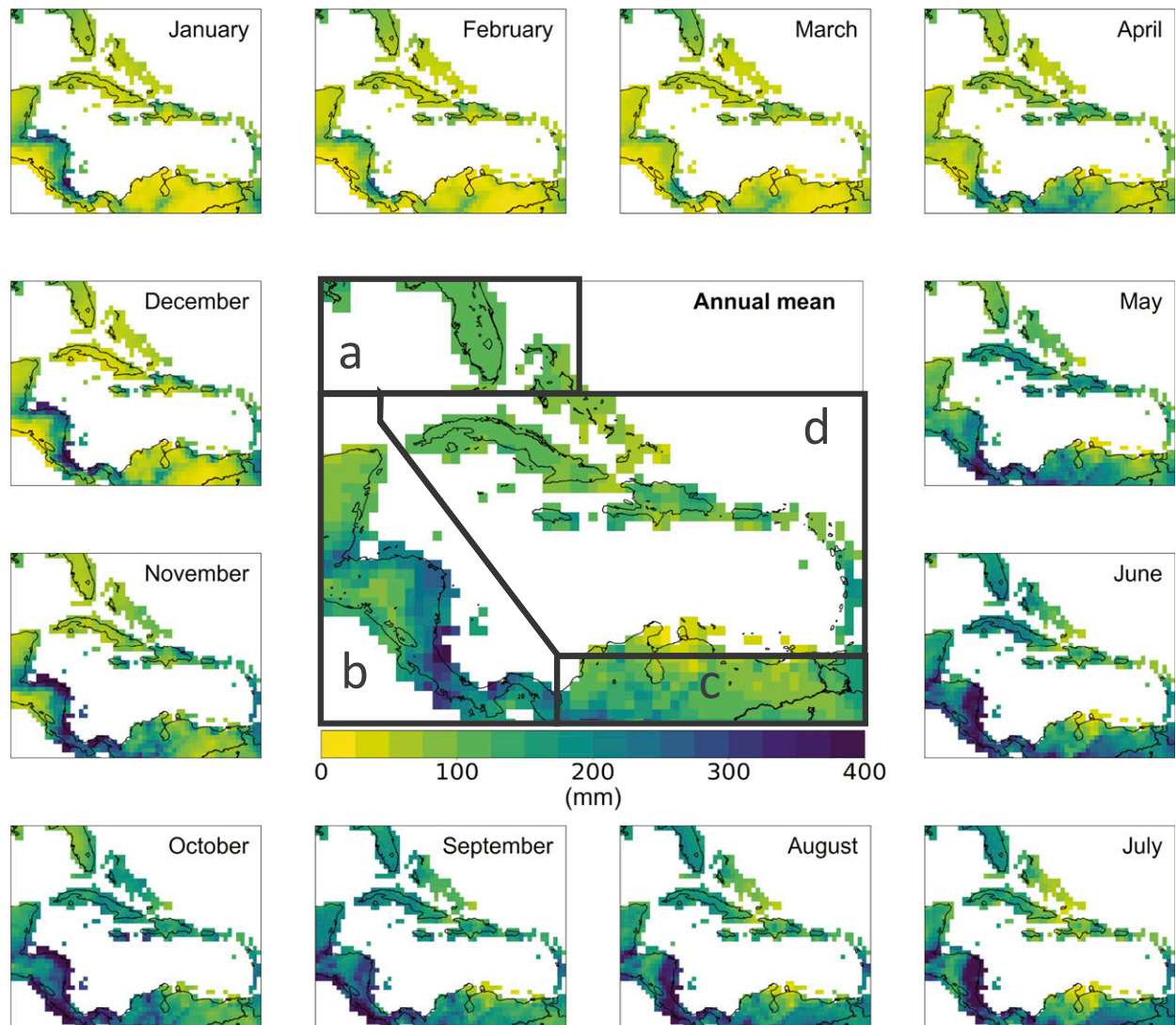


FIG. 1. Monthly precipitation climatology of the study domain (1950–2000) from the GPCP V7 at 0.5° resolution and the annual mean and four focus regions of this work: (a) the Florida Peninsula, (b) Central America, (c) northern South America, and (d) the Caribbean.

selected GPCP V7 for three reasons. First, GPCP data are updated on a regular basis, whereas most similar precipitation datasets (i.e., spanning since at least from 1950 to the near present) are not updated that frequently. This particular feature is essential to further building a high-resolution drought monitoring product for the Caribbean. Second, GPCP V7 has the highest station density in our study domain as compared to other datasets. As shown in Fig. 2, for example, the CRU TS3.24 station density is substantially lower in the Caribbean than in the GPCP V7. Third, GPCP data are one of the most reliable precipitation datasets currently available (Dai and Zhao 2017). For instance, in comparison to scPDSI derived from other precipitation products including the CRU TS3.24, GPCP-data-based scPDSI estimates are more consistent

with other independent drought metrics, such as soil moisture and runoff (Dai and Zhao 2017).

We used the global climate data suite WorldClim (Hijmans et al. 2005; <http://www.worldclim.org/>) and the Climate Hazards Group Infrared Precipitation with Station Data (CHIRPS; Funk et al. 2015) as target fields for downscaling and bias correcting the coarse-resolution temperature and precipitation products described above. WorldClim is a long-term (1950–2000) high-resolution ($\sim 1 \text{ km}^2$ over the equator) global climatology of temperature (T_{\max} , T_{mean} , and T_{\min}) and precipitation, along with other derived bioclimatic variables. The dataset was developed by interpolating long-term monthly climatologies of weather stations using elevation, latitude, and longitude as predictors of

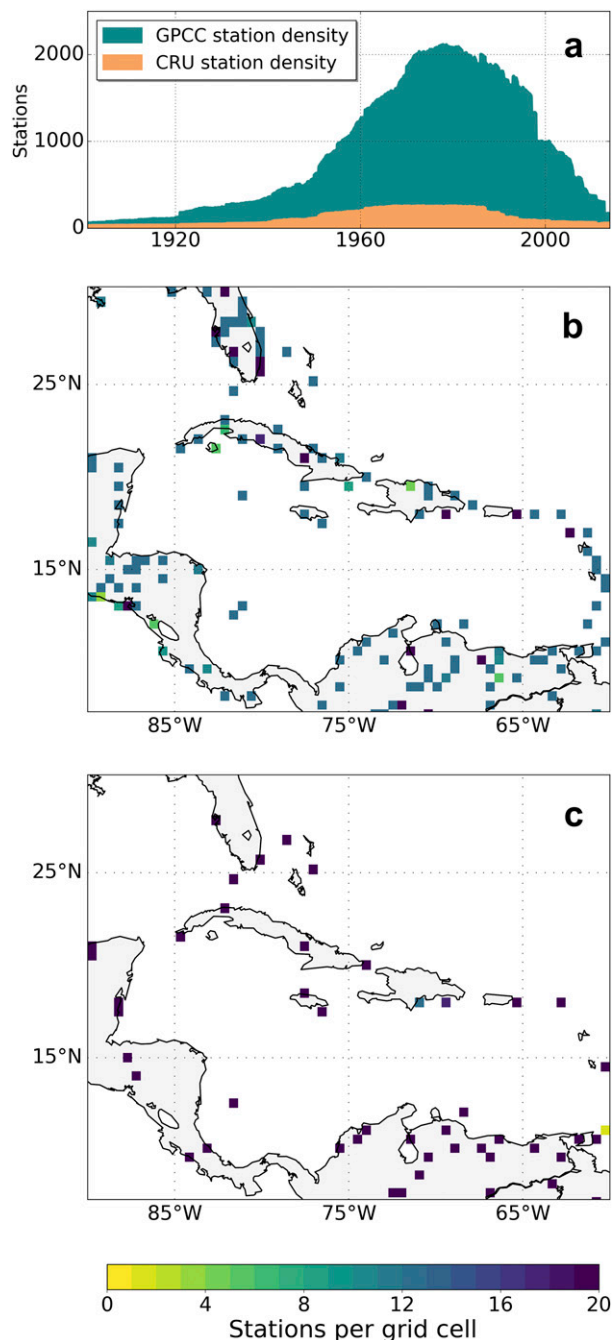


FIG. 2. Number of stations used by GPCCC V7 and CRU TS3.24 in our study domain: (a) station density time series during the 1901–2013 interval, (b) number of station of GPCCC, and (c) CRU TS 3.24 in 2013.

climate variables (Hijmans et al. 2005). WorldClim includes climate data from the GHCN, the Food and Agriculture Organization of the United Nations (FAO), the World Meteorological Organization (WMO), the International Center for Tropical Agriculture (CIAT),

and other additional minor databases from Central and South American countries (as well as others outside the study region) (Hijmans et al. 2005). Despite the scarcity of weather stations with high-quality climate data across our study domain, WorldClim used a relatively dense station network by incorporating climatological data from various sources, as well as by selecting stations with at least 10 years of monthly climate data during the 1950–2000 interval (Hijmans et al. 2005). For example, we estimated that WorldClim used approximately 5000 weather stations¹ (for both temperature and precipitation) in our study domain, mainly distributed over northern South America. However, those stations are not exempt from the problem of missing data; they simply satisfy the minimum requirement of having at least 10 years of climate data to be included in WorldClim. In spite of these obvious limitations, WorldClim is one of the very few high-resolution gridded climatologies currently available that make possible downscaling coarse temperature and precipitation datasets in regions with limited or missing continuous high-resolution data.

Because WorldClim solely provides high-resolution climatologies, we further used CHIRPS to correct monthly biases in variances and means of GPCCC V7. This product spans from 1981 to the present, with a native resolution of 0.05° (~ 6 km) in the Caribbean. It integrates satellite imagery data with in situ weather station data from 50°S to 50°N . As with reanalysis and the GPCCC monitoring product, CHIRPS is updated on a monthly basis with the purpose of drought monitoring (Funk et al. 2015). The number of stations used by CHIRPS to calibrate satellite precipitation estimates in our study domain is currently about 540,² although this number was greater a decade or so ago. Most of the stations currently in use are concentrated in a portion of northern South America and the Florida Peninsula.

The available water holding capacity (AWC) data required for computing the scPDSI were obtained from the Global Gridded Surfaces of Selected Soil Characteristics of the International Geosphere–Biosphere Programme Data and Information Services (IGBP-DIS), through the Oak Ridge National Laboratory (ORNL; <http://daac.ornl.gov/>). This database provides information of various derived soil surfaces, including AWC, soil field capacity, and soil bulk density. It uses a statistical bootstrapping method to generate those

¹ See <https://databasin.org/maps/new#datasets=15a31dec689b4c958ee491ff30fccc75>.

² See ftp://ftp.chg.ucsb.edu/pub/org/chg/products/CHIRPS-2.0/diagnostics/chirps-n-stations_byCountry/.

surfaces from the FAO–United Nations Educational, Scientific and Cultural Organization (UNESCO) Digital Soil Map of the World (Global Soil Data Task Group 2000). Although the native resolution of this product is 5 arc min, we preprocessed using a bilinear interpolation routine to regrid the AWC data to a spatial resolution of 4 km.

b. Methods

For the purpose of facilitating the analysis of scPDSI trends and spatial variability, we divided the study area into four smaller regions based on physiographical settings (e.g., continentality vs insularity) and the total annual precipitation amount: 1) the Florida Peninsula (Fig. 1a), 2) Central America (Fig. 1b), 3) northern South America (Fig. 1c), and 4) the Caribbean (Fig. 1d). Previous studies have suggested dividing the Caribbean into smaller regions based on climatic features such as seasonality (e.g., Giannini et al. 2000; Jury et al. 2007). We, however, examined the Caribbean as a single region because our domain not only includes the islands of the Caribbean, but also Central America and small portions of South and North America. We therefore compare hydroclimatic variations in the Caribbean along with other regions in our domain over the 1950–2016 interval.

1) STATISTICAL DOWNSCALING AND BIAS CORRECTION

As previously mentioned, climate data products used in this work have native spatial resolutions ranging from 0.5° to 2.5° in latitude/longitude. At such scales, variations in drought related to local topography cannot be resolved. In the Caribbean Sea, on islands like Hispaniola or Puerto Rico the spatial distribution and variances of precipitation are strongly conditioned by their highly complex topography (e.g., Izzo et al. 2010), with vertical gradients of up to 2700 m over just 15 km of horizontal distance. For reference, a 1° grid cell roughly covers an area larger than Puerto Rico (~9000 km²). Accordingly, we applied statistical methods to downscale the coarse-resolution reanalysis, GPCC V7, and BEST datasets, as well as to correct biases in means and variances of downscaled fields. Furthermore, we selected a target resolution of 4 km to downscale climate data to make our product comparable with other high-resolution drought monitoring products, such as the West Wide Drought Tracker (<https://wrcc.dri.edu/wwdt/current.php?folder=spi3®ion=ww>), which is forced with the Parameter-Elevation Relationships on Independent Slopes Model (PRISM) gridded datasets (Daly et al. 2002, 2008).

The downscaling method applied in this work is similar to the “delta method” implemented by Mosier et al.

(2014). To downscale temperature, we first calculated the anomalies of the BEST dataset at its native resolution (1° in latitude/longitude). Anomalies of maximum, minimum, and mean monthly temperatures were calculated with respect to the 1950–2000 climatology because the same period was used to construct the WorldClim temperature products. These anomalies were then bilinearly interpolated to match with the target spatial resolution of 4 km. Finally, anomalies were added to the WorldClim climatologies to generate downscaled temperature products with a spatial resolution of 4 km. It was necessary to regrid WorldClim to match our target resolution of 4 km because its native resolution is about 1 km at the equator (Hijmans et al. 2005). Since there are no high-resolution datasets of temperature to correct biases in spatial variances in the Caribbean (as there are for North America), we used the WorldClim temperature seasonality product to adjust annual seasonality of downscaled temperature fields, so they match the WorldClim annual cycle.

WorldClim temperature “seasonality” is the standard deviation of monthly means with respect to the annual average of temperature. We adjusted the annual cycle of our downscaled temperature products following a similar method as suggested by Leander and Buishand (2007):

$$T_{\text{corr}} = \bar{T}_{\text{raw}} + \left[\frac{\sigma(T_{\text{obs}})}{\sigma(T_{\text{raw}})} \right] (T - \bar{T}_{\text{raw}}) + (\bar{T}_{\text{obs}} - \bar{T}_{\text{raw}}), \quad (1)$$

where T_{corr} is the corrected temperature, \bar{T}_{raw} is the annual mean temperature of uncorrected temperature data, and \bar{T}_{obs} is the annual mean temperature from observations, which in this study is the mean from WorldClim climatology. The term $\sigma(T_{\text{obs}})$ is the standard deviation of WorldClim climatology (temperature seasonality), while $\sigma(T_{\text{raw}})$ is the annual standard deviation of the uncorrected temperature (i.e., the standard deviation with respect to the annual mean of every single year of the time series), and T is the uncorrected monthly time series of temperature over a specific grid cell. We modified Eq. (1), so that annual means and trends of the original downscaled data are maintained [Eq. (2)]:

$$T_{\text{corr}} = \bar{T}_{\text{raw}} + \left[\frac{\sigma(T_{\text{obs}})}{\sigma(T_{\text{raw}})} \right] (T - \bar{T}_{\text{raw}}). \quad (2)$$

If this step is done using just Eq. (1), we would be detrending downscaled fields by assigning a constant annual mean on each grid cell time series, hence the different formulation of Eq. (2).

Downscaling and bias-correcting of precipitation required a more sophisticated statistical approach than

for temperature. Bias correction using the WorldClim coefficient of variation, as we did for temperature fields, fails to show spatial variations in precipitation not strictly related to local topography. For example, spatial variations in precipitation associated with frontal systems (which are common in the northwestern Caribbean during boreal winter) in areas with little topographic variability (e.g., Florida) are not captured using this method. Furthermore, we found annual variations in precipitation to be much higher than those in temperature. If we adjust downscaled precipitation to have the same coefficient of variation every year, this “correction” would affect the water balance of the scPDSI function, and consequently we might obtain scPDSI values that do not correspond to local conditions.

We applied a two-step statistical downscaling process using the CHIRPS precipitation dataset to correct monthly spatial variances and means of GPCC V7. As the first step, we regridded the original GPCC dataset to match the resolution of CHIRPS (0.05° or ~6 km). We then corrected the variances and means of GPCC V7 so that these statistics matched those of CHIRPS during the overlapping period from January 1981 to December 2015. This step was done using a quantile mapping approach following the method proposed by Panofsky and Brier (1968):

$$P_{\text{corr},i} = F_{\text{obs}}^{-1}[F_{\text{raw}}(P_{\text{raw},i})], \quad \text{for } i = 1, 2, 3, \dots, 12, \quad (3)$$

where $P_{\text{corr},i}$ is the corrected precipitation for month i , $P_{\text{raw},i}$ is the uncorrected precipitation for month i , F_{obs}^{-1} is the inverse cumulative distribution function (CDF) of observations, which in this case is the CHIRPS dataset, and F_{raw} is the corresponding CDF of uncorrected precipitation.

The second step is similar to the procedure we employed for temperature fields. We calculated precipitation anomalies as the fraction of each month with respect to its 1950–2000 climatology. Those anomalies were bilinearly interpolated and then aggregated to the WorldClim climatology to get a final downscaled product of 4 km. Again, it was necessary to regrid WorldClim precipitation climatologies to our target resolution of 4 km. Last, we adjusted downscaled monthly mean values to match WorldClim’s climatology from 1950 to 2000.

2) EVALUATION AND VALIDATION OF DOWNSCALED PRODUCTS

Where available, we used station data from GHCN versions 2 and 3 (V2 and V3), and homogenized weather station data from the Dominican Republic (from Izzo 2011) to evaluate and validate downscaled climate fields. We calculated root-mean-square errors (RMSEs)

between 58 stations and underlying grid cells for precipitation, and 20 stations for temperature. We also computed Pearson correlation coefficients to evaluate whether downscaled products capture interannual station variability.

To evaluate the performance of WorldClim against other similar products in the Caribbean region, we also downscaled precipitation using the newly released (~1 km) data from the Climatologies at High Resolution for Earth’s Land Surface Areas (CHELSA) product (Karger et al. 2016). The CHELSA suite uses a more sophisticated statistical approach than WorldClim to downscale climate fields from the European Centre for Medium-Range Weather Forecasts (ECMWF) interim reanalysis (ERA-Interim; Dee et al. 2011). CHELSA applies an algorithm that includes orographic predictors such as the wind effect, valley exposure, and the planetary boundary layer for downscaling both precipitation and temperature. It further corrects biases of ERA-Interim products using GPCC and GHCN station datasets (Karger et al. 2016).

As an additional test to evaluate the quality of downscaled products, we regridded GPCC V7 and BEST to match our downscaled precipitation and temperature products, respectively, using the “nearest neighbor” method to maintain their original spatial variations.

3) THE SELF-CALIBRATING PALMER DROUGHT SEVERITY INDEX

The PDSI, in its various forms, is the most widely used metric for drought monitoring in North America (Heim 2002; Dai et al. 2004; Dai 2011, 2013). The original PDSI (which we term PDSI-o) consists of a water balance model that uses precipitation and PET as moisture supply and demand terms, respectively, integrated to a simple two-layer soil model (Palmer 1965). This makes the PDSI-o (and its variants) unique among drought indicators in its capacity to account for soil properties (i.e., AWC) to estimate drought severity. In contrast, the standardized precipitation index (SPI; McKee et al. 1993) and the standardized precipitation evapotranspiration index (SPEI; Vicente-Serrano et al. 2010) present alternative drought metrics to the PDSI-o, but are insensitive to underlying soil characteristics. Values of the PDSI-o smaller than -0.5 or greater than 0.5 indicate dry or wet conditions, respectively (Palmer 1965), while absolute values greater than 4 indicate an extreme event. Despite the success of the PDSI-o as a drought metric, it has also been criticized for showing inconsistent results across different climates (e.g., Alley 1984; Guttman et al. 1992; Wells et al. 2004).

Given the shortcomings of PDSI-o, we used the scPDSI, which makes drought severities comparable

across different climate zones by tuning the index to local conditions (Wells et al. 2004). At its core, the scPDSI X_i is calculated as

$$X_i = pX_{i-1} + qZ_i, \quad (4)$$

where X_i is a given month of the index, X_{i-1} is the index of the previous month, p and q are “duration factors” (which represent the importance of autocorrelation), and Z_i is the current moisture anomaly. As in Dai (2011), we used consecutive negative and positive moisture anomalies to calculate duration factors for dry and wet periods, respectively. Further details on how both the PDSI-o and the scPDSI are calculated are provided by Palmer (1965), Alley (1984), Guttman et al. (1992), and Wells et al. (2004).

Independent of the PDSI variant used, the index “calibration period” must be defined, which is the interval used as a benchmark to establish the normal hydroclimatic conditions for a specific location (Palmer 1965; Dai 2011; van der Schrier et al. 2013). Although previous studies have suggested a 1950–80 interval as the optimum calibration period for computing the PDSI to capture the effect of anthropogenic climate change on drought (e.g., Dai and Zhao 2017), we used a 1950–2000 calibration interval to be consistent with the WorldClim climatology.

We arbitrarily set soil moisture initial conditions to have 50% of total AWC in each layer to initialize the calculations. Since the upper layer S_s has a fixed AWC of one inch, its initial moisture content was set at 0.5 in. (1 in. \approx 2.54 cm); moisture content in the lower layer S_u depends on the total AWC as $S_u = \text{AWC} - S_s$ (Palmer 1965). In addition, we calculated the index beginning in January 1949 to minimize the influence of the initial conditions because our analysis spans the period from 1950 to 2016.

4) POTENTIAL EVAPOTRANSPIRATION

In addition to using the self-calibrated version of the PDSI, we followed recent recommendations for “best practices” with the PDSI index (van der Schrier et al. 2011; Smerdon et al. 2015), using the Penman–Monteith (PM) method (Penman 1948; Monteith 1965) for calculating evapotranspiration, rather than the Thornthwaite equation (Thornthwaite 1948) used in PDSI-o. This approach is considered more physically realistic and more appropriate for evaluating the effects of climate change on drought severity (van der Schrier et al. 2011; Smerdon et al. 2015; Williams et al. 2015). Given the limited long-term climate data available for the Caribbean, we applied a variant of the PM that requires fewer climate fields for its computation [Eq. (5)] and is currently

used by the FAO (Allen et al. 1998). Using this method, the PET is calculated as

$$\text{PET} = \frac{0.408\Delta(\text{Rn} - G) + \gamma \frac{900}{T + 273.16} U_2 (e_s - e_a)}{\Delta + \gamma(1 + 0.34U_2)}, \quad (5)$$

where the quantities are defined as follows: PET is the crop reference evapotranspiration (mm day^{-1}), Rn is the net radiation ($\text{MJ m}^{-2} \text{day}^{-1}$), G is the soil heat flux density ($\text{MJ m}^{-2} \text{day}^{-1}$), T is the average temperature at 2-m height ($^{\circ}\text{C}$), U_2 is the wind speed measured (or estimated from U_{10}) at 2-m height (m s^{-1}), U_{10} is the wind speed measured at 10-m height (m s^{-1}), $e_s - e_a$ is the vapor pressure deficit for measurement at 2-m height (kPa), Δ is the slope of the vapor pressure curve ($\text{kPa } ^{\circ}\text{C}^{-1}$), γ is the psychrometric constant ($\text{kPa } ^{\circ}\text{C}^{-1}$), 900 is the coefficient for the reference crop ($\text{kJ}^{-1} \text{kg K day}^{-1}$), and 0.34 is the wind coefficient for the reference crop (sm^{-1}) (Allen et al. 1998). The concept behind this method stands from modeling an idealized grass surface with 0.12-m height, a constant water supply, and a soil resistance of 70 s m^{-1} . It also assumes a surface albedo of 0.23 (Allen et al. 1998). Although previous studies have shown a minimal impact on using either the PM or the Thornthwaite PET estimates for computing the PDSI (e.g., Dai 2011; van der Schrier et al. 2011) over the historical period, we suggest that variables included in the PM method, such as the vapor pressure deficit, might play a critical role on drought severity in the Caribbean during climate change (e.g., Williams et al. 2015).

With the method we used to calculate the PET, five climate variables are required: monthly averages of daily maximum, mean, and minimum temperature (T_{max} , T_{mean} , and T_{min}), wind speed, and cloud cover. We used down-scaled and bias-corrected temperature fields, while the other variables were bilinearly interpolated reanalysis products to match with the target resolution of 4 km. Monthly averages of saturation vapor pressure e_s were estimated from vapor pressure:

$$e(T) = 0.6108 \exp\left(\frac{17.27T}{T + 237.3}\right), \quad (6)$$

where $e(T)$ is the vapor pressure (kPa) as a function of the air temperature, and T is the air temperature in degrees Celsius. To assess potential biases on saturation vapor pressure resulting from the nonlinearity of Eq. (6), we also calculated e_a using daily T_{max} and T_{min} , and then it was averaged to obtain monthly e_a estimates. We found minor differences on using both approaches, yielding a mean difference $< 0.002 \text{ kPa month}^{-1}$. Equation (6) was also applied to calculate the actual vapor pressure e_a , which requires the dewpoint temperature rather than the

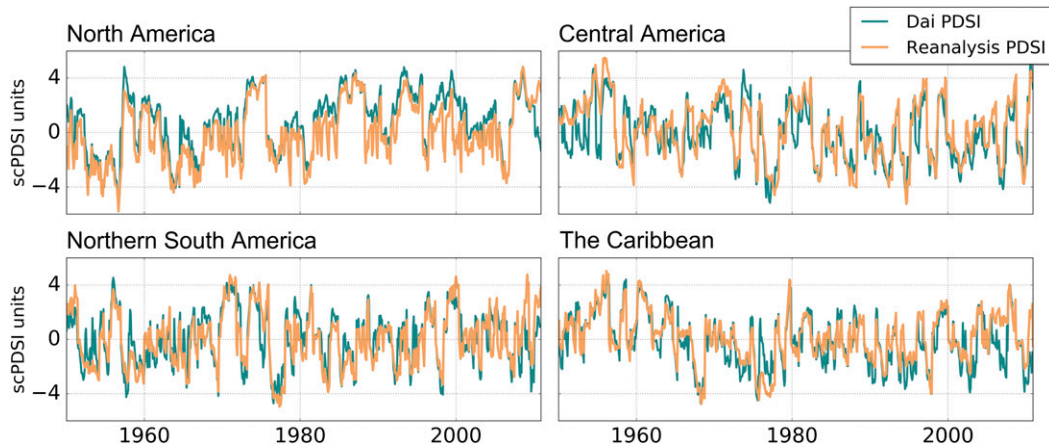


FIG. 3. Comparison between the coarse-resolution PDSI calculated using the NCEP–NCAR reanalysis data (regridded to 1°) and the Dai PDSI dataset (Dai 2011) on few selected grids from North America, Central America, northern South America, and the Caribbean. The “reanalysis PDSI” was computed using the GPCC V7 dataset for precipitation and reanalysis products of temperature, total cloud cover, and wind speed climatology.

air temperature. As suggested by Allen et al. (1998), the minimum temperature can be used to compute e_a when dewpoint temperature and other humidity data are not available. Although there are reanalysis products for both the relative and specific humidity, we derived e_a using our downscaled mean minimum daily temperature in place of the dewpoint temperature because there is not a high-resolution dataset to further correct biases in means and variances of downscaled humidity fields from reanalysis. We also used minimum temperature to be consistent with the saturated vapor pressure, which was calculated using our downscaled temperature products. In addition, uncertainties are high for humidity reanalysis products because they are largely based on simulated data (Kalnay et al. 1996; Williams et al. 2015). A similar approach was applied by Harris et al. (2014) to construct a 0.5° -resolution vapor pressure dataset as part of the CRU TS3.10 climate suite. A caveat of using this approach is that we are assuming the dewpoint temperature is never lower than the minimum temperature, which is not always realistic. However, this is mostly an issue for arid and semiarid regions (Allen et al. 1998). Although in the Caribbean there are few semiarid regions (e.g., southern Hispaniola and northern South America), we found that the method performs fairly well by qualitatively comparing our PET dataset with the CRU PET product.

Net radiation was calculated from reanalysis cloud cover (to derive sunshine hours) following Allen et al. (1998). Although this product has been classified as a category “C” variable, which indicates that it is derived solely from the model without observations (Kalnay et al. 1996), we found that it has a minimal impact on the scPDSI (Fig. 3). Finally, previous studies have reported

major uncertainties in the reanalysis wind speed product because of the limited availability of high-quality observations (e.g., Dai 2011). To partially address this issue, we used the long-term wind speed monthly climatologies rather than the entire dataset, as in van der Schrier et al. (2013) with the CRU wind speed product. As with cloud cover, we compared the scPDSI forced with wind speed climatology, obtaining similar trends and variances of that in the Dai (2011) scPDSI dataset (Fig. 3).

5) LONG-TERM TRENDS AND DROUGHT RANKING

We calculated long-term trends in the scPDSI using the best-fit linear least squares method. Trends with p values greater or equal to 0.05 at the 95% confidence level were not considered in our analysis, although they are also described in the results. We calculated linear trends over the study area, as well as in each of the regions we divided our domain to identify changes at regional scales. Furthermore, given the strong autocorrelation of the scPDSI, we also calculated trends of the Palmer’s moisture anomaly index (Z index; Palmer 1965) to contrast them against scPDSI trends. The Z index has very little (if any) autocorrelation and can serve as benchmark to assess the significance of the trends in the scPDSI.

To estimate the area where the recent 2013–16 drought was record breaking, we ranked droughts by selecting the smallest monthly scPDSI values in each grid cell time series. In our analysis, the lower the ranking value the more severe the drought. That is, the most severe drought will be ranked as number one, while the wettest period of the same time series will occupy the last position.

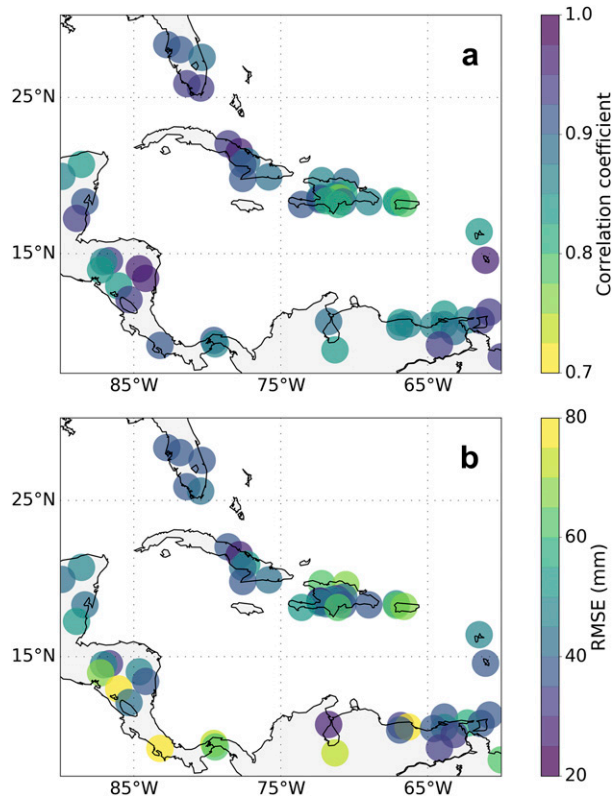


FIG. 4. (a) Correlation coefficients and (b) RMSEs between our downscaled precipitation product and GHCN station data. We selected GHCN stations with at least 15 years with continuous data during the 1950–2016 interval.

6) SEA SURFACE TEMPERATURE

To identify large-scale climate patterns associated with Caribbean drought, we used the Extended Reconstructed Sea Surface Temperature, version 4 (ERSST.v4), dataset (Huang et al. 2015; Liu et al. 2015) to correlate sea surface temperature anomalies (SSTAs) with the scPDSI across the study domain. Correlations were done with SSTA averaged over the Niño-3.4 region (5°N – 5°S , 170° – 120°W) in the tropical Pacific and with the tropical North Atlantic (0° – 20°N , 60° – 20°W) because these regions have been linked to the natural variability of precipitation in our study domain (e.g., Enfield and Alfaro 1999; Giannini et al. 2000, 2001a,b; Taylor et al. 2002; Jury et al. 2007). We further correlated regionally averaged scPDSI from our drought atlas with global SSTA to gain insights into the linkages between drought and remote patterns of SST variability. Since previous studies have shown seasonal changes in correlations between precipitation and SSTA from both tropical Pacific and North Atlantic (Giannini et al. 2000, 2001a,b; Taylor et al. 2002; Jury et al. 2007), we also conducted seasonal correlations using two seasons: 1) the early rainy season of May–July

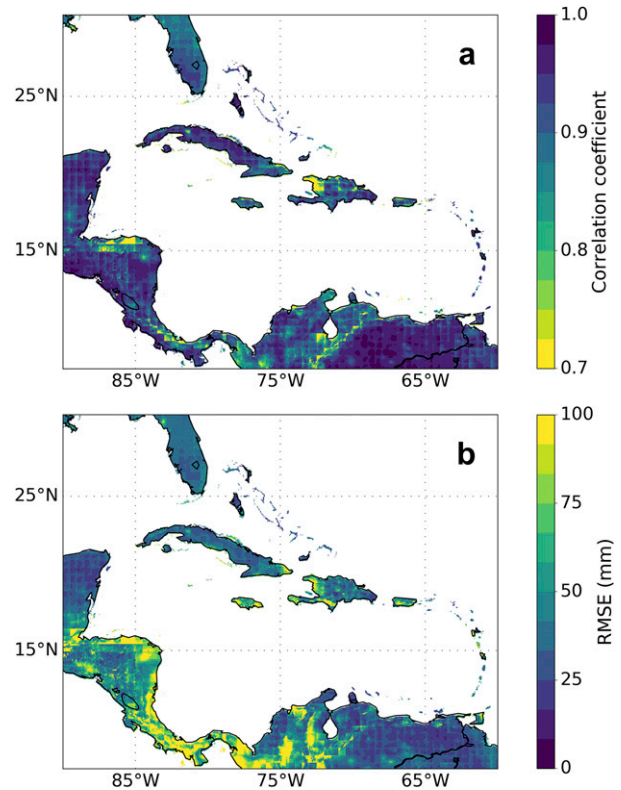


FIG. 5. (a) Correlation coefficients and (b) RMSEs between our downscaled precipitation product and the GPCC V7 interpolated to 4 km (using the nearest-neighbor method) during the 1950–2016 interval. The largest biases are observed over Central America and the Andes in South America.

(MJJ), and 2) the late rainy season of August–October (ASO).

3. Results

a. Validation of downscaled products

Correlation coefficients between downscaled monthly precipitation and GHCN station vary from 0.76 to 0.97, with an average of 0.89 over the study domain (Fig. 4a). The lowest correlations are found in the Caribbean and western Central America, as well as over coastal stations in northern South America (Fig. 4a). In terms of RMSE, the lowest value is 27 mm in the Maracaibo–Los Pozos station in Venezuela, while the highest is 79 mm in Caucagua, Venezuela (Fig. 4b). Both RMSEs account for less than 60% of the station standard deviation. Furthermore, correlations between the GPCC V7 re-gridded product and our downscaled precipitation product (4 km) average over 0.92. Lower correlations are found on grids over the Andes in northern South America and Hispaniola (Fig. 5a).

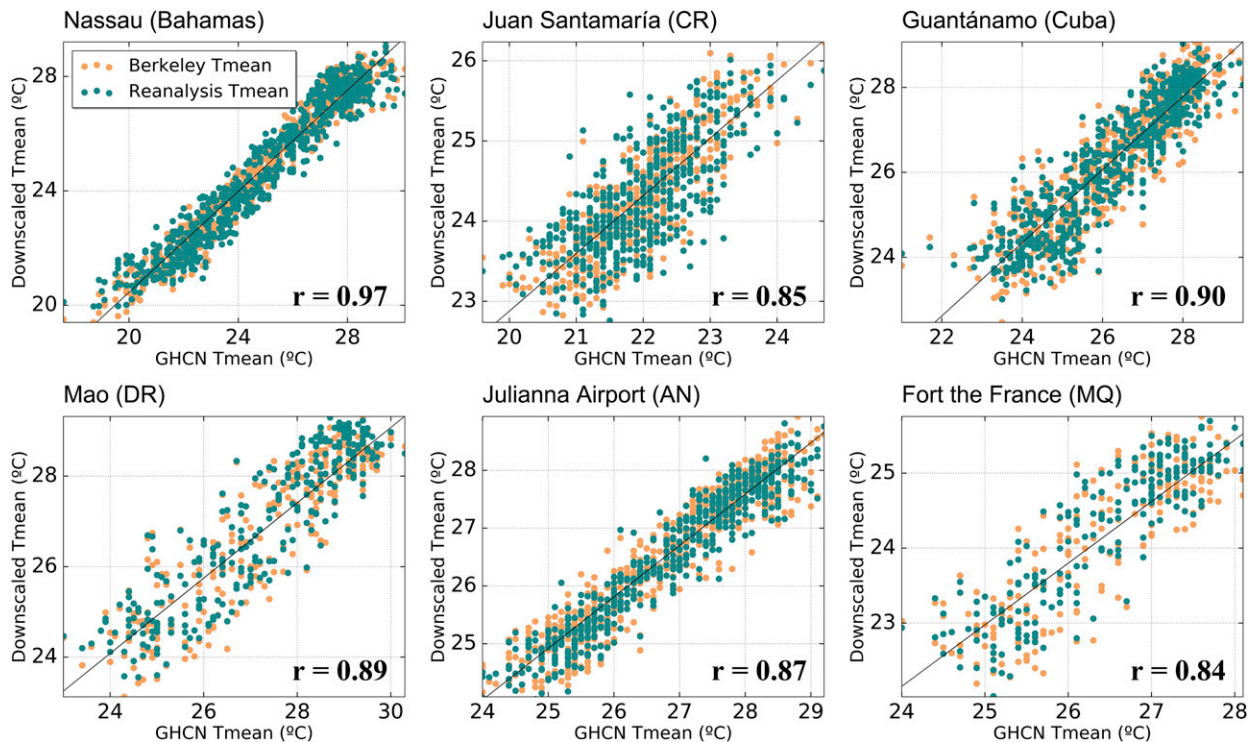


FIG. 6. Scatterplots of monthly mean temperatures of six GHCN stations and downscaled data from BEST (brown) and reanalysis (cyan) data during the 1950–2016 interval. We selected weather stations with at least 10 years without missing data located in the Bahamas, Costa Rica (CR), Cuba, Dominican Republic (DR), Netherlands Antilles (AN), and Martinique (MQ, France). The values of both axes differ in each panel because of differences in the average temperature among stations. Diagonal lines in each panel represent the 1:1 correlation line.

Correlation coefficients and RMSE values between our BEST-downscaled temperature fields (T_{\max} , T_{mean} , and T_{\min}) and GHCN station data are similar to those of precipitation (Fig. 6). The higher biases in mean temperature are found over mountainous regions in Central America (RMSE = 1.08°C), Hispaniola (RMSE = 0.91°C), and northern South America (RMSE = 0.89°C). The same pattern is also apparent in monthly minimum and maximum temperature means, with RMSE ranging from 0.79° to 1.12°C. Similar correlations and RMSE are found between our reanalysis-downscaled temperature products and GHCN.

Downscaled BEST-based and reanalysis-based temperature products are very similar despite their differing spatial scales and underlying methodological assumptions (Fig. 6). Overall, correlations and RMSE are 0.88 and 0.40°C, respectively, with the highest biases in northern South America, where correlations are below 0.6. However, grid cells with correlations below 0.85 only represent 20% of the study domain. Downscaled BEST products also correlate slightly better with some GHCN stations, as compared to downscaled reanalysis temperature products. For example, BEST mean

temperature has a higher correlation ($r = 0.85$) than reanalysis ($r = 0.78$) with the Juan Santamaria Airport station in Costa Rica.

The minor differences between BEST and reanalysis temperatures are also noticeable in the potential evapotranspiration. As shown in Fig. 7, both products perform similarly over the Caribbean and Central America. The largest biases are found, again, over northern South America, especially in the Orinoco River basin and the Andes (Fig. 7). Moreover, correlations between the BEST-based PET and reanalysis-based PET during the 1980–2016 interval (used as a benchmark of the satellite era) are lower than those calculated using the entire time series from 1950 to 2016 (Figs. 7c,d).

b. WorldClim versus CHELSA downscaled precipitation

While WorldClim and CHELSA climatologies might reflect somewhat different mean climate states because of their differing temporal coverage (1950–2000 vs 1979–2013, respectively), we assume that major features such as rain shadows and regional spatial variations in

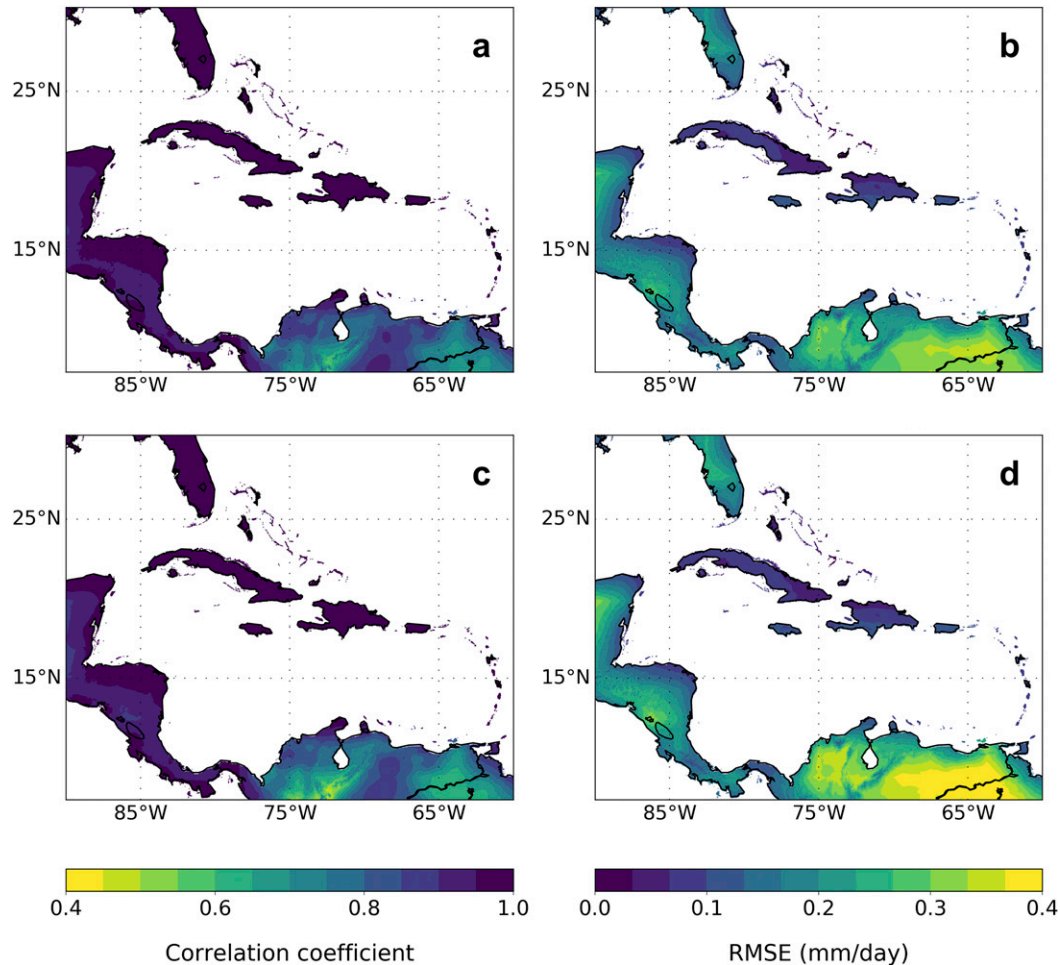


FIG. 7. (a),(c) Correlation coefficients and (b),(d) RMSEs between PET calculated using BEST and NCEP-NCAR reanalysis surface temperature products. Lower correlations were observed over northern South America, while the highest RMSEs were also observed on the same region. Note that (a) and (b) show correlations and RMSE, respectively, using the full time series (from 1950 to 2016), while (c) and (d) are the same metrics as computed after 1980 to assess the skill of reanalysis for the satellite era.

precipitation are maintained over time. Overall, both downscaled precipitation products show similar long-term and spatial variances, as assessed using correlation coefficients and RMSE (Fig. 8). Averaged total annual precipitation differ in terms of their spatial variances, with the WorldClim-downscaled precipitation showing slightly higher contrast in rain shadows than with the CHELSA product. These differences are more noticeable in the Caribbean (particularly on Hispaniola) and Central America (Fig. 8). However, in spite of these differences, the averaged correlation between both products is 0.94.

CHELSA and WorldClim scPDSI estimates also show similar long-term trends and variations. Minor differences, mainly in the timing of some droughts and pluvials (i.e., the beginning and the end of dry and wet

intervals), are observed in areas of complex topography in Central America and the Caribbean.

c. Major droughts and pluvials during the 1950–2016 interval

1) MAJOR DROUGHTS

The worst droughts during the 1950–2016 interval (Fig. 9) were identified from the perspective of Caribbean islands (region in Fig. 1d). That is, we spatially averaged scPDSI over the Caribbean region and then selected the droughts using a scPDSI ≤ -1.5 threshold, with at least one year in duration. Because of this, major droughts identified in the Caribbean might not be the most extreme dry intervals in other regions such as northern South America, the Florida Peninsula, or

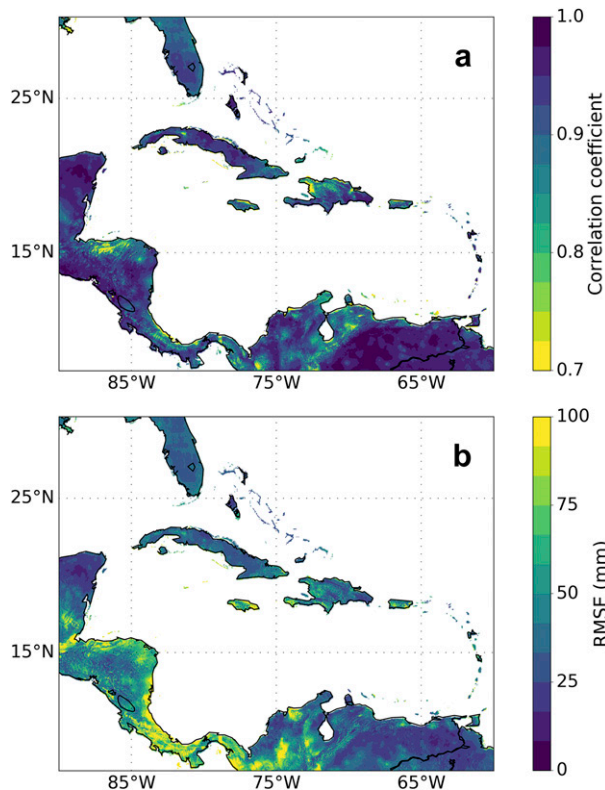


FIG. 8. (a) Correlation coefficients and (b) RMSEs between downscaled precipitation products using WorldClim and CHELSA. Both downscaled products span the 1950–2016 interval.

Central America (Fig. 9), and in some instances they may not be correlated at all, as shown in Table 2.

We identified the first major drought in the Caribbean between 1974 and 1977. It was one of the most widespread and prolonged dry intervals in this region, and affected 49% of the study domain (as calculated from the percentage of grid cells with $\text{scPDSI} \leq -1$) and 70% of the Caribbean (Figs. 9 and 10). In terms of severity, we calculated averaged scPDSI of -1.1 in the study domain (and much lower values locally), -1.5 in the Caribbean, -0.4 in northern South America, -0.6 in Central America, and -1.4 in the Florida Peninsula (Fig. 9). Localized wetter conditions occurred in the Andean region of northern South America, with scPDSI values indicating a slight wet spell (~ 1.0).

The 1997/98 drought (Fig. 9) occurred during the strong El Niño of 1997/98. Although dry conditions intensified across the region in the summer of 1997, they persisted until the summer and autumn of 1998. About 49% and 16% of the study area were affected by mild ($-1 \geq \text{scPDSI} \geq -1.9$) and severe ($-3 \geq \text{scPDSI} \geq -3.9$) drought conditions, respectively (Figs. 9 and 10), while at least 50% of the Caribbean was under mild drought (Fig. 10). Regions particularly affected by this event

were northern South America, with a regional scPDSI average of -1.6 , Central America (-1.4 scPDSI), and the Caribbean (-0.8 scPDSI). In contrast to the 1974–77 dry interval, the Florida Peninsula experienced slightly wetter conditions during the 1997/98 drought, with a regional scPDSI of 0.8.

Between mid-2009 and late 2010, a severe and widespread drought once again affected the domain, especially northeastern South America, the Caribbean (mostly the Lesser Antilles), and portions of Central America (Fig. 9). During this event, 68% of the study area was under mild drought conditions, and 28% was under severe drought (Fig. 10). Furthermore, over 85% of northern South America as well as 99% of the Lesser Antilles were severely affected by the drought (Fig. 10). In contrast to other major droughts in the Caribbean, this dry interval did not appreciably affect the Greater Antilles, with approximately 59% of land area under mild drought conditions. In terms of severity, regional scPDSI averages vary across the study domain, from -0.9 scPDSI in the Caribbean to -3.0 in South America. For the rest of the regions, scPDSI averaged -1.5 in Central America and 0.4 in the Florida Peninsula.

More recently, between late 2013 and early 2016, the Caribbean and most of the study domain further struggled with a severe drought. As in the 1997/98 period, part of this period occurred during a strong El Niño. However, this drought was considerably more severe and widespread, affecting 80% of the study area, and almost 95% of the Caribbean with a mild drought (Figs. 9 and 10). The drought peaked in 2015, and during this year almost the entire Caribbean was experiencing mild drought conditions, while 51% of the islands were in severe drought (Fig. 10). In terms of regional averages, this drought reached scPDSI of -2.6 in the Caribbean, -3.1 in northern South America, and -2.2 in Central America. In contrast, Florida Peninsula received above normal precipitation, with a mean scPDSI of 0.8 (a similar pattern to the 1997/98 drought). However, unlike the 1997/98 drought, the 2013–16 event affected the southern portion of the Florida Peninsula (Fig. 9), as well as northwestern Cuba.

2) MAJOR PLUVIALS

Major pluvials were selected by repeating the method to choose major droughts in the Caribbean. We found that some pluvials coincided with active hurricane seasons in the North Atlantic, including those in 1979, 2008, and 2012. A brief analysis of this result is provided in section 4b. Furthermore, it was found that very wet conditions (i.e., $\text{scPDSI} \geq 3$) occur on more localized scales as compared to severe droughts (i.e., $\text{scPDSI} \leq -3$), at least in the Caribbean (Fig. 11).

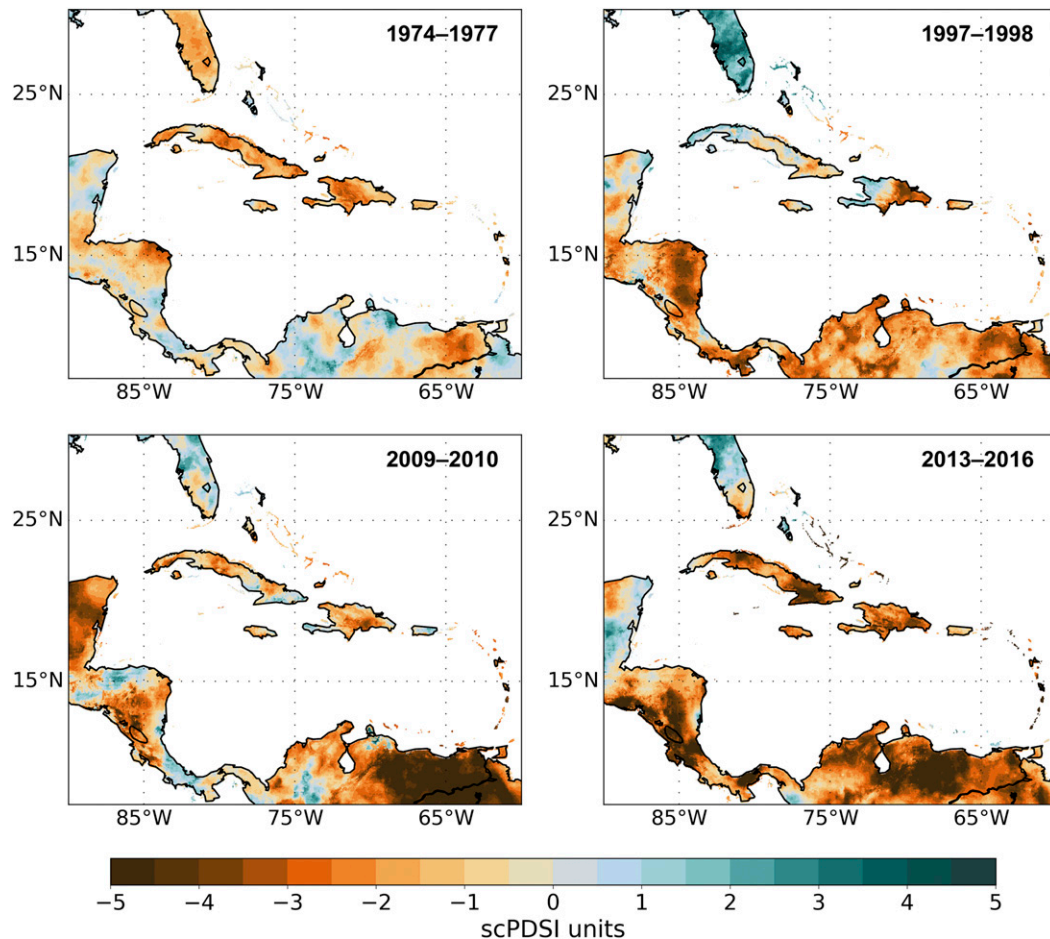


FIG. 9. Major droughts registered in the study area from the perspective of the Caribbean between 1950 and 2016 of at least one year in duration.

One of the most prominent pluvials occurred between 2012 and 2013 (Fig. 11), when 60% of our domain and 50% of the Caribbean were under wet conditions ($\text{scPDSI} \geq 1$) (Fig. 12). We calculated a regionally averaged scPDSI of 1.4, which is considered slightly wet (Palmer 1965). This wet interval was most pronounced in northern South America, with a regionally averaged scPDSI of 2.9. Furthermore, most of the Caribbean and the Pacific coast of Central America experienced mild wet conditions as well, with a mean scPDSI of 1.9 and 1.3, respectively. In contrast, the Florida Peninsula and the Caribbean coast of Central America were experiencing a moderate drought, with an average scPDSI of -2.0 .

Other major pluvials also occurred during 1958–62, 1977–81, and 2007–09, but they were not as widespread as the 2012/13 wet period. In some cases, a “seesaw pattern” between northern South America and the Florida Peninsula is particularly pronounced, where pluvials in one region are usually paired with dry conditions in the other, and vice versa (Fig. 11). During the

wet periods in 1958–62, 1977–81, and 2007–09, 27%, 51%, and 59%, respectively, of the study domain was under slightly wet conditions (Fig. 12).

d. Long-term trends

Linear trends in the scPDSI vary markedly across the study area, even at local scales (Fig. 13). We calculated scPDSI trends during the 1950–2008 interval to compare our results with trends previously reported by

TABLE 2. Correlations between spatially averaged scPDSI time series of the regions shown in Fig. 1. Boldface numbers indicate a statistically significant correlation ($p < 0.05$) at the 95% level.

| | Central America | Northern South America | Caribbean |
|------------------------|-----------------|--------------------------|-----------|
| Florida Peninsula | -0.3 | -0.5 | 0.06 |
| Central America | — | 0.7 | 0.46 |
| Northern South America | — | — | 0.4 |

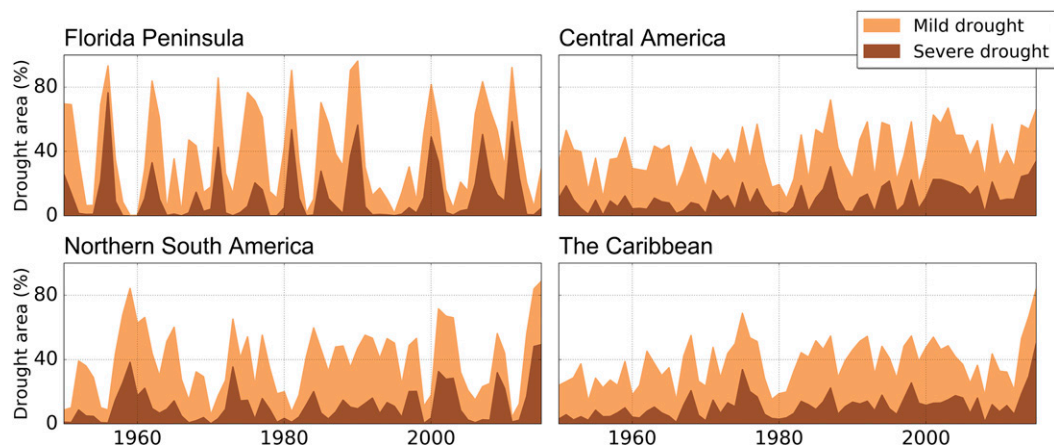


FIG. 10. Drought area index time series of the four focus regions used in this work, calculated based on the percentage of grid cells with $scPDSI \leq -1$ (mild drought) and with $scPDSI \leq -3$ (severe drought).

Dai (2011) in the Caribbean (Fig. 13a). In general, results reveal a statistically significant decline in the $scPDSI$ —indicating a drying trend—from 1950 to 2008 ($p < 0.05$), with an average trend of $-0.09 scPDSI decade^{-1}$.

It is important to mention, however, that this is the spatially averaged trend across the study area, which means that in specific locations drying trends are more pronounced. Sectors of Central America (e.g., in Nicaragua

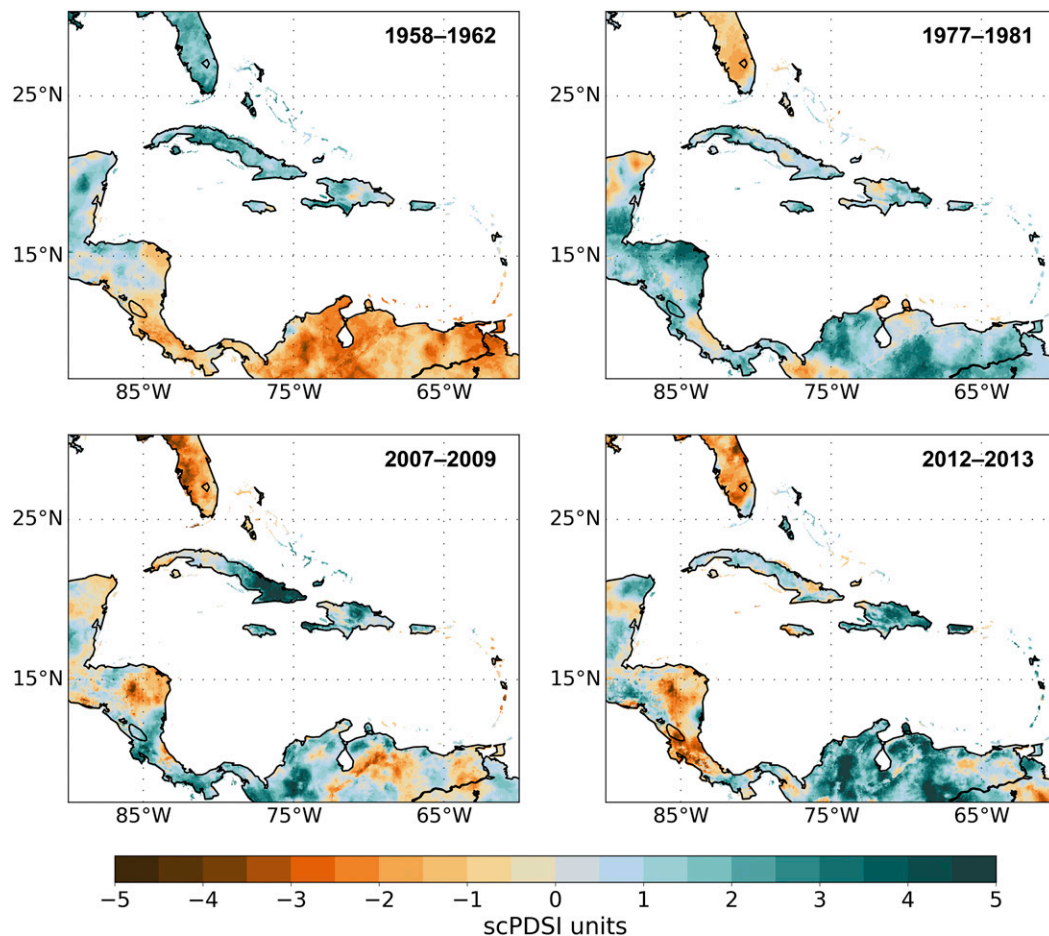


FIG. 11. As in Fig. 9, but for pluvials.

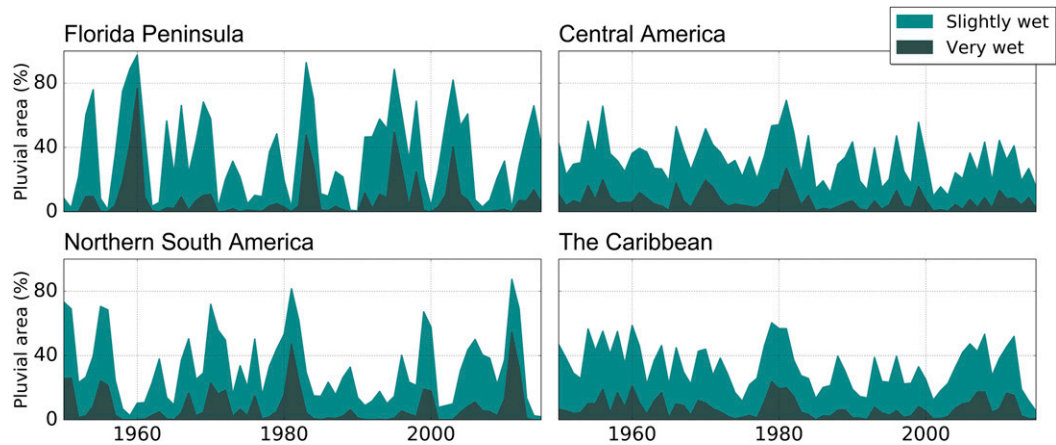


FIG. 12. As in Fig. 10, but for pluvials.

and Honduras), for example, have linear trends of -0.25 scPDSI decade $^{-1}$ ($p < 0.05$) (Fig. 13a).

We further calculated linear trends including the full time interval of our drought product (1950–2016), which depict a similar pattern as from 1950 to 2008 (Fig. 13b). Differences were observed in the intensity of the trends, but in general the spatial patterns were consistent. Significant positive trends prevailed in northern South America (10°N , 75°W) with scPDSI trends averaging 0.15 scPDSI decade $^{-1}$ ($p < 0.05$). Positive trends were also found in Puerto Rico (average change of 0.15 scPDSI decade $^{-1}$) and the highlands of Hispaniola (average change of 0.07 scPDSI decade $^{-1}$) but they were not statistically significant ($p = 0.12$). A similar result was also observed in the trends of the Z index, although they are slightly lower than those in the scPDSI (± 0.04 units decade $^{-1}$).

REGIONAL TRENDS

Regional trends calculated using the full interval of 66 yr are shown in Fig. 14. As with our selection of the worst dry and wet intervals, we spatially averaged the scPDSI over the regions we divided our study domain. Results reveal that scPDSI declined significantly in three of the four regions, with the highest drying trend in northern South America with -0.1 scPDSI decade $^{-1}$ ($p < 0.05$). The linear trend in northern South America is closely followed by trends in the Caribbean (-0.09 scPDSI decade $^{-1}$; $p < 0.05$) and Central America (-0.087 scPDSI decade $^{-1}$; $p < 0.05$). Although results also indicate a drying trend in the Florida Peninsula (-0.06 scPDSI decade $^{-1}$), this is not statistically significant ($p = 0.15$).

e. Sea surface temperature correlations

Seasonal correlations between SSTA and scPDSI time series vary during seasonal cycles (Fig. 15). Negative

correlations associate above-normal SST with drought, and positive correlations with wetter conditions. For example, Fig. 15 shows the correlations between scPDSI in the Caribbean with global SSTA during MJJ. A nonstatistically significant correlation is observed with the tropical Pacific region during this season ($r = -0.2$), while it is significant over the tropical North Atlantic ($r = 0.5$). In contrast, during ASO (Fig. 15) both oceanic basins are significantly correlated with scPDSI in the Caribbean ($r \approx \pm 0.5$). Furthermore, correlation patterns between SSTAs and the Florida Peninsula scPDSI are quite the opposite from those observed in the Caribbean, Central America, and northern South America (Fig. 15). This region is significantly correlated with the tropical Pacific in both seasons, while a nonstatistically significant correlation is observed with the tropical North Atlantic (Fig. 15).

4. Discussion

a. Evaluation of downscaling and bias-correction methods

Our drought atlas underscores the advantage of using high-resolution climate products for calculating the scPDSI in insular regions like the Caribbean. This is not only because high-resolution datasets allow us to evaluate variations in drought at local scales, but also because the smallest insular states in the region are resolved. For example, some of the Lesser Antilles do not appear in the current drought datasets (e.g., Dai et al. 2004; Dai 2011; Vicente Serrano et al. 2010; van der Schrier et al. 2013), simply because those islands are much smaller than a single grid cell of such products. From our drought atlas, islands even smaller than 100 km^2 (such as some of the British Virgin Islands) are represented. Furthermore, we assessed the consistency

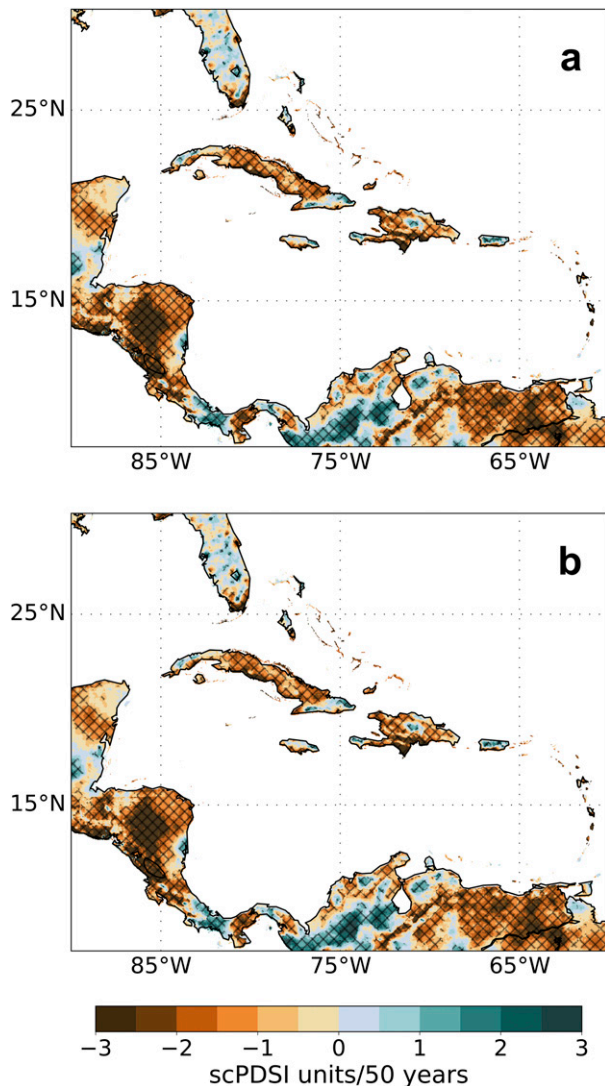


FIG. 13. Linear trends showing (a) the change of the scPDSI during the 1950–2016 interval and (b) in 1950–2008. Brown colors represent a drying trend, and cyan colors a wetting trend. In (a) and (b), the hatching means a significant trend ($p < 0.05$) at the 95% level.

of our drought product with two approaches. First, we used statistical tools to compare the forcing climate datasets—especially precipitation—with station data before calculating the scPDSI. Even though correlation coefficients may not fully capture the differences among datasets, we ensured a more realistic comparison by combining correlations with RMSE. Both approaches indicate that our downscaled products are consistent with station data in terms of trends and variability. Second, we contrasted our drought atlas with reports issued by local public institutions describing some of their historical droughts. We compared, for example, spatial variations of the recent 2013–16 drought in

Puerto Rico in our atlas against reports issued by the Puerto Rican Department of Natural and Environmental Resources (DRNA). In these reports, the evolution of the drought was documented using various indicators, including the United States Drought Monitor (USDM; <http://droughtmonitor.unl.edu>), and precipitation anomalies estimated from satellite products (DRNA 2016). Although some biases were observed in our drought atlas, especially in the western side of the island, it captured the persistent drought in southern Puerto Rico as described in those reports.

We found that the delta method implemented here is appropriate in light of limitations in high-resolution gridded climate products in our study region, and for being computationally inexpensive. A key advantage of this method is the relatively low volume of climate data required for its implementation, as compared to more sophisticated statistical methods like bias-corrected constructed analogs (BCCA; Maurer et al. 2010) or bias correction and spatial disaggregation (BCSD; Wood et al. 2004). For example, while ideally it might be better to downscale using BCCA (because of its sophisticated statistical approach), high-resolution historical products are required for the constructed analog (CA) step used in this method. This issue in particular prevented us from applying such a method. While BCCA and BCSD require high-resolution climate datasets, the delta method used here only needs high-resolution climatologies of the variables to downscale. This is especially important for the Caribbean because there is no a single high-resolution product that resolves for local topography from 1950 to near-present. Although CHIRPS may be used to downscale precipitation using the BCSD method, it only spans from 1981 to the present, and we required consistency in our downscaling approach for both temperature and precipitation going back to 1950.

b. Characteristics of droughts and pluvials

The eight extreme events we analyzed help us to characterize some key features of dry and wet intervals in our study area. For example, spatial variations in drought are characterized by a seesaw pattern between northern South America and the Florida Peninsula, where droughts in northern South America are accompanied by wet periods in Florida, and vice versa (e.g., Figs. 9 and 11). This pattern is particularly apparent with droughts and pluvials during ENSO events, and it is also observed when comparing the drought area index in each region (Fig. 10). During the 1997/98, 2009/10, and 2013–16 droughts in northern South America and the Caribbean, wetter conditions prevailed in the Florida Peninsula, and in some cases in western Cuba (Fig. 9). These findings are consistent with previous studies (e.g., Schultz et al. 1998; Giannini et al. 2001a,b) in which

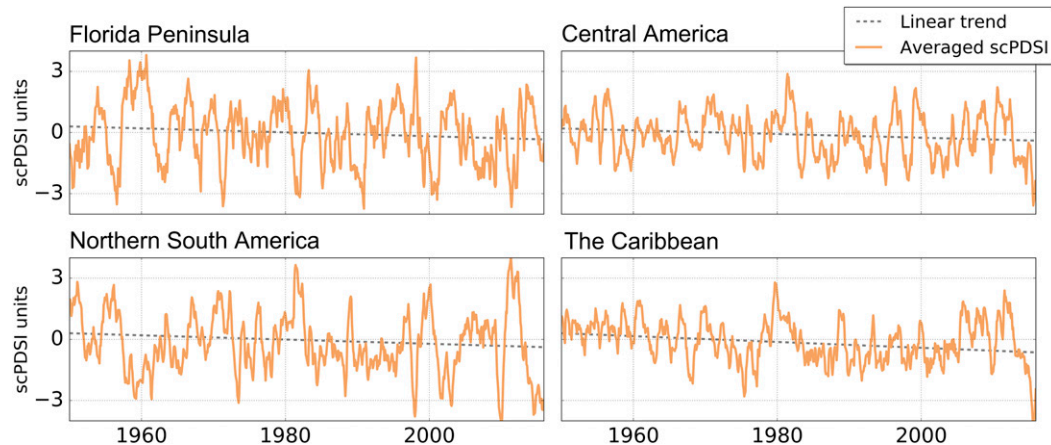


FIG. 14. Linear trends of spatially averaged scPDSI over the four key regions. Note the seesaw pattern between the Florida Peninsula and northern South America.

warm phases of the ENSO have been associated with drought in northern South America, and above-normal precipitation in the Florida Peninsula. The wetter conditions observed in Florida correlate with a higher intrusion of frontal systems during the boreal winter when El Niño peaks. In contrast, a persistent subsidence over northern South America could be responsible for the drier conditions observed during El Niño in this region (Giannini et al. 2001a,b).

Some pluvials occurred during active hurricane seasons in the North Atlantic. Although the scPDSI smooths the influence of extreme precipitation events like those associated with tropical cyclones, we examined some of the most intense hurricanes that affected Hispaniola in 1979, 1998, and 2008. In some instances, like after Hurricanes David (1979) and Georges (1998), we found scPDSI changes of 1.6 and 1.8, respectively, in a single month. Hispaniola was also affected by two tropical cyclones in August 2008, including Hurricane Gustav. Averaged scPDSI across the island changed from -1.8 in July 2008 (mild drought conditions) to 2.9 in August (moderately wet), representing a change of 4.2 scPDSI in one month. Although tropical cyclones last for a few days, they often bring substantial amounts of precipitation (on the order of hundreds of millimeters in few days) that eventually contribute to a major change in the scPDSI, even in a short period of time. For example, the greatest accumulated monthly precipitation in Barahona (Dominican Republic, during 1939–2008) is 945 mm (Izzo 2011).³ This extreme event occurred in October 1963 and coincided with the

landfall of major Hurricane Flora in southwestern Hispaniola. In fact, this amount is 7 times the average precipitation for October in this station (~ 160 mm) and virtually equal to its annual mean (~ 950 mm). As estimated from Roth (2008), the contribution of Flora to this event was approximately 800 mm, or roughly 85% of total precipitation in this month. These results highlight the role that tropical cyclones might play in ending droughts or worsening pluvials at local scales in the Caribbean. However, based on these findings we cannot argue that pluvials in the Caribbean are solely caused by the natural variability of tropical cyclones. Hence, this warrants further research that might include dynamical downscaling of landfalling hurricanes in the region to provide insights into the possible interplay between tropical cyclones and local topography in modulating drought variability.

Our atlas is also consistent with previous studies connecting SSTA to drought variability in the region (e.g., Enfield and Alfaro 1999; Giannini et al. 2000, 2001a,b; Taylor et al. 2002; Jury et al. 2007). As shown in Fig. 15, regional scPDSI time series are significantly correlated with SSTA, especially in the tropical Pacific and North Atlantic Oceans. However, correlation patterns with indices from these basins vary across the study area, and are even anticorrelated. For example, while scPDSI in the Florida Peninsula is positively correlated with above normal tropical Pacific SSTs, the correlations are negative in Central America, northern South America, and the Caribbean (Fig. 15). This means that during El Niño events, wetter conditions are usually observed in Florida and drought observed in the rest of the domain. These findings are also consistent with the seesaw pattern seen in the most extreme hydroclimatic intervals, and highlight the influence of both the tropical

³ Station data provided by the National Meteorological Office of the Dominican Republic (ONAMET).

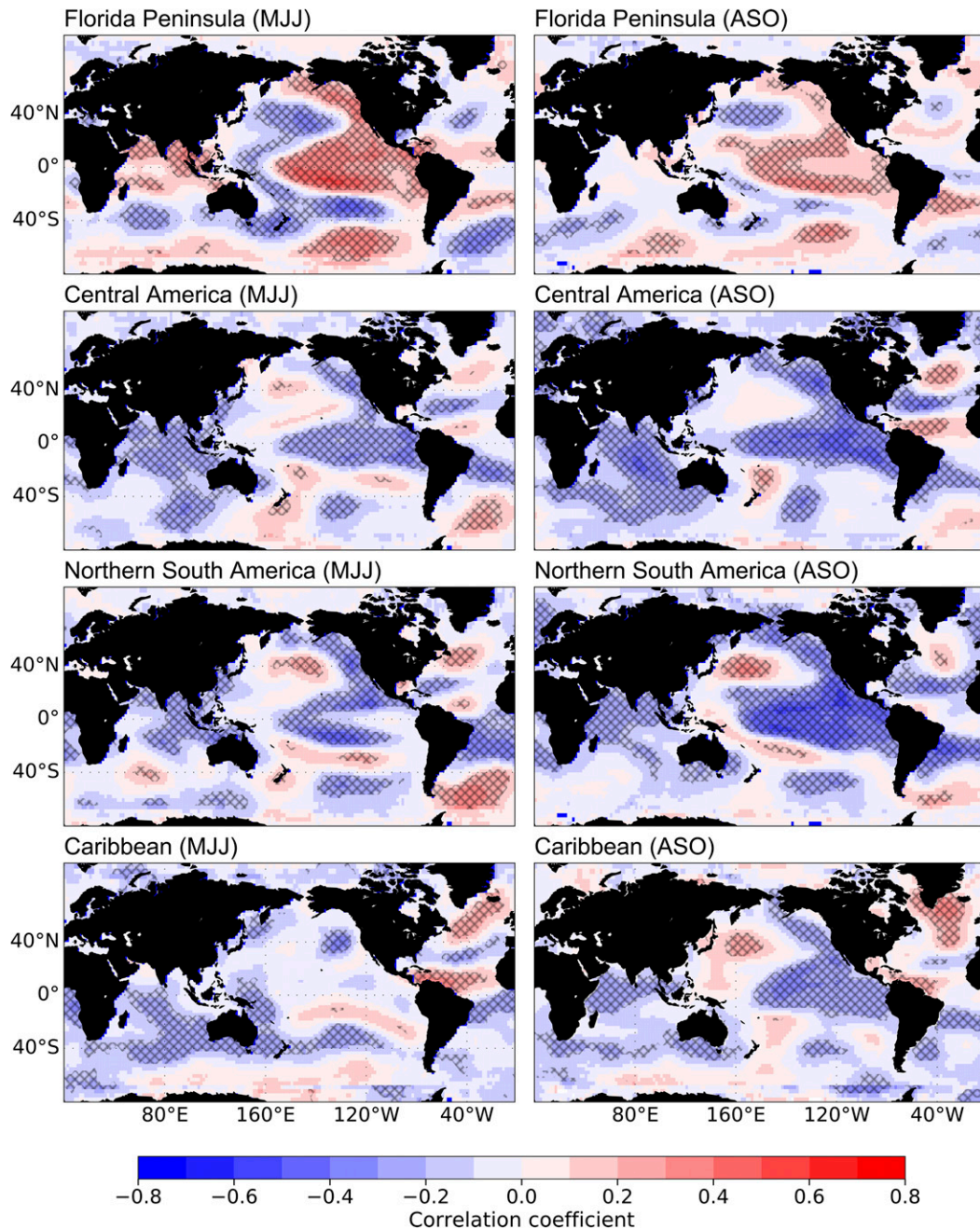


FIG. 15. Seasonal correlations between regionally averaged scPDSI time series in our study domain and global SSTAs during the 1950–2016 interval. The hatched areas are statistically significant correlations at the 95% level.

Pacific and North Atlantic in modulating drought variability in our study area. Furthermore, correlations not only vary across space but also through the seasonal cycle. For example, scPDSI in the Caribbean is significantly correlated with the tropical Pacific during early boreal autumn (ASO), while there is no correlation in boreal spring–summer (MJJ) (Fig. 15). In contrast, the same region is positively correlated with the tropical

North Atlantic in both seasons, which means that above normal temperature in this sector of the North Atlantic ocean is usually associated with higher precipitation in the Caribbean (e.g., Giannini et al. 2000, 2001a,b; Taylor et al. 2002; Jury et al. 2007).

Correlations further vary at local scales across the study domain, and even in the same region. Regionally averaged scPDSI in Central America is, for example,

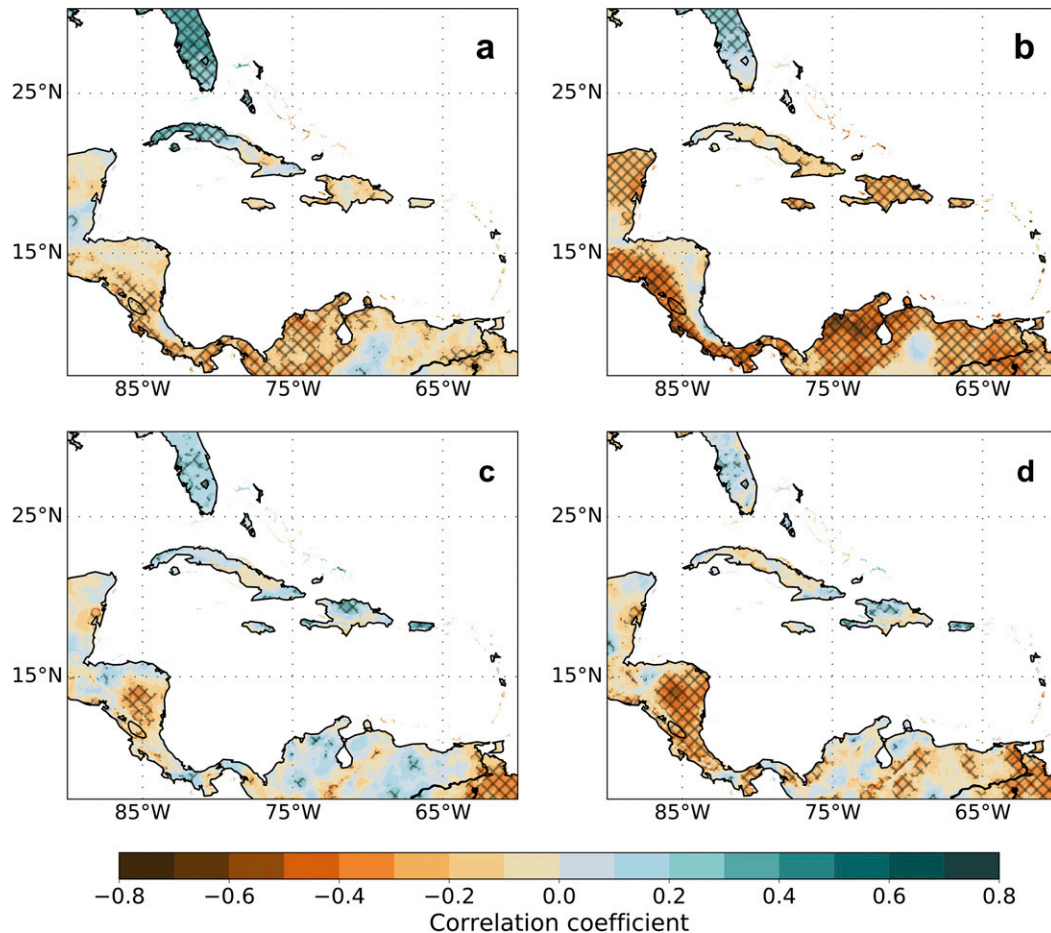


FIG. 16. Correlations between scPDSI and SSTAs over the Niño-3.4 region during the (a) MJJ and (b) ASO periods. (c),(d) As in (a),(b), but with SSTAs over the tropical North Atlantic. The hatched areas are statistically significant correlations at the 95% level.

negatively correlated with the tropical Pacific (Fig. 15), but this pattern is not equally strong across the region (Fig. 16). The Pacific coast of Central America appears to be more sensitive to variations in the Niño-3.4 region, while the Caribbean coast is not correlated at all ($p > 0.05$), and indeed positive correlations are observed in some grid cells (Fig. 16). Similarly, statistically significant correlations are observed in western Cuba with the Niño-3.4 during MJJ, while the eastern side of the island is negatively correlated. These patterns suggest the role topography might have in modulating drought variation in our study domain by modulating the spatial variation of precipitation.

c. The 2013–16 Caribbean drought

Results from this work indicate that during the 2013–16 interval, the Caribbean faced the most severe and widespread drought since 1950. This drought has caused major water shortages in agriculture, municipal

consumption, and energy generation,⁴ mainly affecting Hispaniola, Cuba, Puerto Rico, and Jamaica, as well as the Lesser Antilles. We call this dry interval a “pan-Caribbean drought” because virtually all Caribbean islands were affected by it. As the Caribbean, Central America, and northern South America also confronted serious problems with water shortage in agriculture and municipal consumption due to this drought.

The drought was record breaking in the summer of 2015, when 99% of the Caribbean, 98% of northern South America, and 87% of Central America were under drought conditions (Fig. 17). In terms of severity, it was also record breaking in 17% of the domain in 2015. These findings indicate that this event was not only the most severe in terms of scPDSI values (below -6 scPDSI in the

⁴ See <http://reliefweb.int/disaster/dr-2015-000091-hti>.

Caribbean and Central America) but it was also the most widespread drought since at least 1950.

El Niño has been identified as the culprit of some major droughts in the Caribbean, Central America, and northern South America (e.g., [Giannini et al. 2000](#), [2001a,b](#); [Taylor et al. 2002](#); [Jury et al. 2007](#)), including the 1997/98 and the recent 2013–16 event ([Amador et al. 2016](#)). However, as compared to the 1997/98 drought, when even northwestern Cuba and Florida experienced wetter conditions, the 2013–16 dry interval was extremely dry in both locations. This aridity not only extended across the entire island of Cuba, but also affected portions of Florida that usually receive above normal precipitation during El Niño ([Giannini et al. 2001a,b](#)). Other particular difference between these “El Niño droughts” was their duration. Whereas the 1997/98 event lasted a year, the 2013–16 drought extended for at least three years, since it is still (at the time of writing) ongoing in some locations of the study area.⁵

To assess the potential role of temperature anomalies on this anomalous drought, we ranked annual PET anomalies using our PET product. We found the highest anomalies in both PET and temperatures in 2015, which coincides with the driest year in the Caribbean during the 2013–16 drought ([Fig. 18](#)). We therefore argue that temperature anomalies during the drought might have been a major contributor to the severity of this event, in addition to lower precipitation. Nevertheless, further studies are required to fully evaluate the details of this picture.

5. Conclusions

We have documented the first high-resolution scPDSI-based drought atlas for the Caribbean and Central America, spanning 1950–2016. We argue that high-resolution drought products are required for the Caribbean region, not only because of its complex topography and inherent insularity, but also because of its unique exposure to the impacts of climate change across these gradients. This atlas delivers critical information to researchers and stakeholders by providing insight into the historical backdrop of drought variability in the region. This is especially important for the Caribbean, since many of its nations have been recognized as some of the most vulnerable countries to severe droughts and pluvials ([Stephenson et al. 2014](#), [2016](#)). We summarize the main findings of this work as follows:

- Downscaling and bias-correction methods applied in this work are robust in capturing spatial and temporal

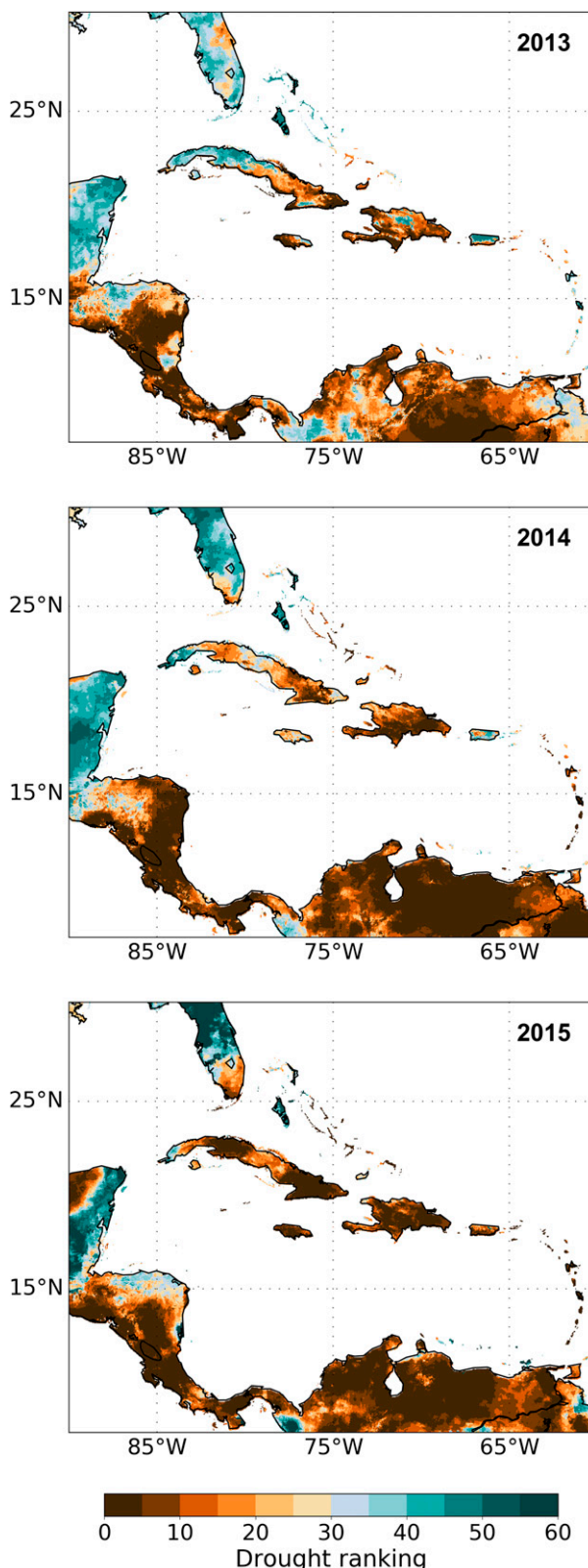


FIG. 17. Annual drought rankings between 2013 and 2015. Drought conditions in 2014 ranked as the most severe since 1950 in a greater area than in 2015. However, in the Caribbean, 2015 ranks as the driest year during the 2013–16 drought.

⁵ See <http://rcc.cimh.edu.bb/spi-monitor-january-2017/>.

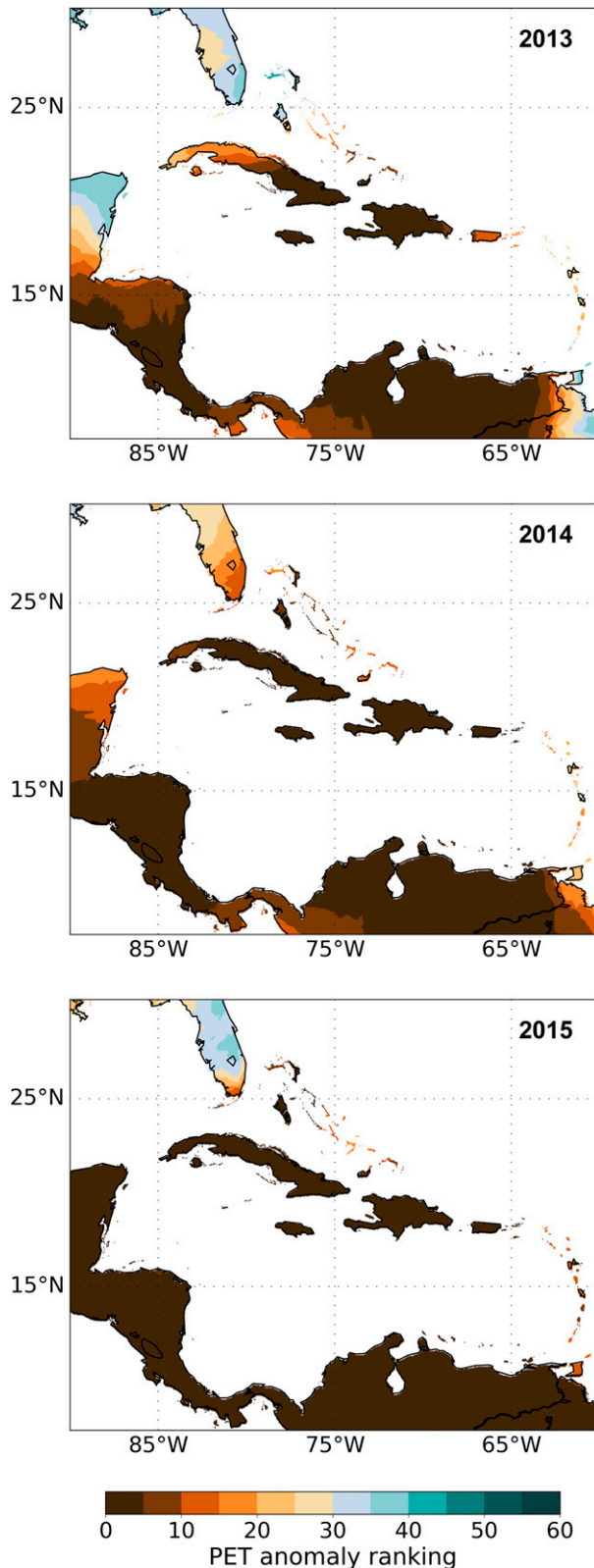


FIG. 18. As in Fig. 17, but for annual PET anomalies.

variations of the underlying climate data. For example, correlations and root-mean-square errors indicate that our downscaled products capture the interannual variability of stations, as well as major droughts and pluvials. Furthermore, comparing the scPDSI derived from station-based precipitation and temperature records against our downscaled fields shows that these two approaches yield consistent results.

- A seesaw pattern in droughts and pluvials is observed between the Florida Peninsula and northern South America. These findings are consistent with previous studies (Giannini et al. 2000, 2001a,b; Taylor et al. 2002; Jury et al. 2007) but have not been documented at such high spatial resolution until now. Likewise, both the tropical Pacific and North Atlantic appear to have the highest influence in modulating drought variations in our study domain.
- Linear trends in the scPDSI vary substantially across the study area, and even at local scales. For example, in general, a significant drying trend is prevalent in the Caribbean ($-0.09 \text{ decade}^{-1}$, $p < 0.05$) whereas a wetting trend is observed in the highlands of Hispaniola and Puerto Rico (0.15 decade^{-1} , $p \geq 0.05$). Regional trends in Central America, northern South America, and the Florida Peninsula also show a predominant drying trend. We also found that, even though trends in the scPDSI across the study area are tied to the decline in precipitation, the increasing trend in temperature might also have a substantial effect.
- Finally, the 2013–16 Caribbean drought is the worst multiyear period of aridity in the Caribbean and Central America since at least 1950. It was both more severe and more extensive than any other event in our dataset. This dry interval appears to be related not only to El Niño-driven precipitation deficits, but also to temperature-driven increases in PET. Furthermore, our results agree with station-based reports from many meteorological institutions across the Caribbean that recognized the 2013–16 drought as the worst event in decades, or even in the last 100 years in some countries.

In conclusion, we consider this effort to be the first step in building a high-resolution drought product for the Caribbean and Central America that can be updated regularly, and made available to the public for ongoing monitoring and modeling efforts. Further applications of this atlas could include quantifying potential predictability across multiple temporal or spatial scales, targeting it for paleoclimate reconstructions, or applying rigorous detection and attribution analysis to the historical trends. Regardless, our results document—for the first time, to our knowledge—that the 2013–16 drought was indeed the worst on record in terms of both

its severity and spatial extent since at least 1950. Future work could therefore help clarify the contribution of anthropogenic warming to this extreme anomaly, as well as help constrain future risks in a changing climate.

Acknowledgments. This material is based upon work partially supported by a National Science Foundation EaSM2 Grant (AGS-1243125), and National Science Foundation Grant AGS-1602564. GHCN V2 and V3 time series used in this work were obtained from the Koninklijk Nederlands Meteorologisch Instituut (KNMI) Climate Explorer (<https://climexp.knmi.nl/>). The authors further acknowledge the Fulbright Scholar Program for partially supporting this work.

REFERENCES

- Allen, R., and Coauthors, 1998: Crop evapotranspiration: Guidelines for computing crop water requirements. FAO Irrigation and Drainage Paper 56, 300 pp.
- Alley, W. M., 1984: The Palmer Drought Severity Index: Limitations and assumptions. *J. Climate Appl. Meteor.*, **23**, 1100–1109, doi:10.1175/1520-0450(1984)023<1100:TPDSIL>2.0.CO;2.
- Amador, J. A., H. G. Hidalgo, E. J. Alfaro, A. M. Durán-Quesada, and B. Calderón, 2016: Regional climates: Central America and the Caribbean [in “State of the Climate in 2015”]. *Bull. Amer. Meteor. Soc.*, **97**, S178–S181, doi:10.1175/2016BAMSStateoftheClimate.1.
- Ault, T. R., J. E. Cole, J. T. Overpeck, G. T. Pederson, and D. M. Meko, 2014: Assessing the risk of persistent drought using climate model simulations and paleoclimate data. *J. Climate*, **27**, 7529–7549, doi:10.1175/JCLI-D-12-00282.1.
- , J. S. Mankin, B. I. Cook, and J. E. Smerdon, 2016: Relative impacts of mitigation, temperature, and precipitation on 21st-century megadrought risk in the American Southwest. *Sci. Adv.*, **2**, e1600873, doi:10.1126/sciadv.1600873.
- Blunden, J., and D. S. Arndt, Eds., 2016: State of the Climate in 2015. *Bull. Amer. Meteor. Soc.*, **97**, S1–S275, doi:10.1175/2016BAMSStateoftheClimate.1.
- Campbell, J. D., M. A. Taylor, T. S. Stephenson, R. A. Watson, and F. S. Whyte, 2011: Future climate of the Caribbean from a regional climate model. *Int. J. Climatol.*, **31**, 1866–1878, doi:10.1002/joc.2200.
- Cook, B. I., J. E. Smerdon, R. Seager, and S. Coats, 2014: Global warming and 21st century drying. *Climate Dyn.*, **43**, 2607–2627, doi:10.1007/s00382-014-2075-y.
- , T. R. Ault, and J. E. Smerdon, 2015: Unprecedented 21st century drought risk in the American Southwest and Central Plains. *Sci. Adv.*, **1**, e1400082, doi:10.1126/sciadv.1400082.
- , E. R. Cook, J. E. Smerdon, R. Seager, A. P. Williams, S. Coats, D. W. Stahle, and J. V. Díaz, 2016: North American megadroughts in the Common Era: Reconstructions and simulations. *Wiley Interdiscip. Rev.: Climate Change*, **7**, 411–432, doi:10.1002/wcc.394.
- Dai, A., 2011: Characteristics and trends in various forms of the Palmer Drought Severity Index during 1900–2008. *J. Geophys. Res.*, **116**, D12115, doi:10.1029/2010JD015541.
- , 2013: Increasing drought under global warming in observations and models. *Nat. Climate Change*, **3**, 52–58, doi:10.1038/nclimate1633.
- , and T. Zhao, 2017: Uncertainties in historical changes and future projections of drought. Part I: Estimates of historical drought changes. *Climatic Change*, doi:10.1007/s10584-016-1705-2, in press.
- , K. Trenberth, and T. Qian, 2004: A global dataset of Palmer Drought Severity Index for 1870–2002: Relationship with soil moisture and effects of surface warming. *J. Hydrometeorol.*, **5**, 1117–1130, doi:10.1175/JHM-386.1.
- Daly, C., W. P. Gibson, G. H. Taylor, G. L. Johnson, and P. Pasteris, 2002: A knowledge-based approach to the statistical mapping of climate. *Climate Res.*, **22**, 99–113, doi:10.3354/cr022099.
- , and Coauthors, 2008: Physiographically sensitive mapping of temperature and precipitation across the conterminous United States. *Int. J. Climatol.*, **28**, 2031–2064, doi:10.1002/joc.1688.
- Dee, D. P., and Coauthors, 2011: The ERA-Interim reanalysis: Configuration and performance of the data assimilation system. *Quart. J. Roy. Meteor. Soc.*, **137**, 553–597, doi:10.1002/qj.828.
- DRNA, 2016: Informe sobre la sequía de 2014–2016 en Puerto Rico. Departamento de Recursos Naturales y Ambientales del Estado Libre Asociado de Puerto Rico (DRNA), División de Monitoreo del Plan de Aguas, San Juan, Puerto Rico, 92 pp.
- Enfield, D. B., and E. J. Alfaro, 1999: The dependence of Caribbean rainfall on the interaction of the tropical Atlantic and Pacific Oceans. *J. Climate*, **12**, 2093–2103, doi:10.1175/1520-0442(1999)012<2093:TDOCRO>2.0.CO;2.
- FAO, 2016: Situation report: Dry corridor in Central America. Food and Agriculture Organization of the United Nations, 3 pp. [Available online at <http://www.fao.org/emergencies/resources/documents/resources-detail/en/c/422097/>.]
- Funk, C., and Coauthors, 2015: The climate hazards infrared precipitation with stations—A new environmental record for monitoring extremes. *Sci. Data*, **2**, 150066, doi:10.1038/sdata.2015.66.
- Giannini, A., Y. Kushnir, and M. Cane, 2000: Interannual variability of Caribbean rainfall, ENSO, and the Atlantic Ocean. *J. Climate*, **13**, 297–311, doi:10.1175/1520-0442(2000)013<0297:IVOCRE>2.0.CO;2.
- , M. A. Cane, and Y. Kushnir, 2001a: Interdecadal changes in the ENSO teleconnection to the Caribbean region and the North Atlantic Oscillation. *J. Climate*, **14**, 2867–2879, doi:10.1175/1520-0442(2001)014<2867:ICITET>2.0.CO;2.
- , J. C. Chiang, M. A. Cane, Y. Kushnir, and R. Seager, 2001b: The ENSO teleconnection to the tropical Atlantic Ocean: Contributions of the remote and local SSTs to rainfall variability in the tropical Americas. *J. Climate*, **14**, 4530–4544, doi:10.1175/1520-0442(2001)014<4530:TETTTT>2.0.CO;2.
- Global Soil Data Task Group, 2000: Global Gridded Surfaces of Selected Soil Characteristics (IGBP-DIS). Distributed Active Archive Center, Oak Ridge National Laboratory, doi:10.3334/ORNLDAAC/569.
- Guttman, N. B., J. R. Wallis, and J. R. M. Hosking, 1992: Spatial comparability of the Palmer Drought Severity Index. *J. Amer. Water Resour. Assoc.*, **28**, 1111–1119, doi:10.1111/j.1752-1688.1992.tb04022.x.
- Harris, I., P. D. Jones, T. J. Osborn, and D. H. Lister, 2014: Updated high-resolution grids of monthly climatic observations: The CRU TS3.10 dataset. *Int. J. Climatol.*, **34**, 623–642, doi:10.1002/joc.3711.
- Heim, R. R., 2002: A review of twentieth-century drought indices used in the United States. *Bull. Amer. Meteor. Soc.*, **83**, 1149–1165, doi:10.1175/1520-0477(2002)083<1149:AROTDI>2.3.CO;2.

- Hijmans, R. J., S. E. Cameron, J. L. Parra, P. G. Jones, and A. Jarvis, 2005: Very high resolution interpolated climate surfaces for global land areas. *Int. J. Climatol.*, **25**, 1965–1978, doi:10.1002/joc.1276.
- Holding, S., D. M. Allen, S. Foster, A. Hsieh, I. Larocque, J. Klassen, and S. C. Van Pelt, 2016: Groundwater vulnerability on small islands. *Nat. Climate Change*, **6**, 1100–1103, doi:10.1038/nclimate3128.
- Howitt, R. E., J. Medellín-Azuara, D. MacEwan, J. R. Lund, and D. Sumner, 2014: Economic analysis of the 2014 drought for California agriculture. Tech. Rep., Center for Watershed Sciences, University of California, Davis, 20 pp. [Available online at <https://watershed.ucdavis.edu/2014-drought-report/>]
- Huang, B., and Coauthors, 2015: Extended Reconstructed Sea Surface Temperature version 4 (ERSST.v4): Part I. Upgrades and intercomparisons. *J. Climate*, **28**, 911–930, doi:10.1175/JCLI-D-14-00006.1.
- IMN, 2016: Pronóstico: Fenómeno ENOS y estación lluviosa 2016. Instituto Meteorológico Nacional de Costa Rica (IMN), San José, Costa Rica, 14 pp. [Available online at <https://www.imn.ac.cr/web/imn/43/>]
- IPCC, 2014: *Climate Change 2014: Synthesis Report*. R. K. Pachauri and L. A. Meyer, Eds., IPCC, 151 pp.
- Izzo, M., 2011: Analisi del clima e delle dinamiche climatiche nella Repubblica Dominicana e delle relative influenze sul territorio. Ph.D. thesis, University of Molise, Italy, 162 pp.
- , C. M. Rosskopf, P. P. C. Aucelli, A. Maratea, R. Méndez, C. Pérez, and H. Segura, 2010: A new climatic map of the Dominican Republic based on the Thornthwaite classification. *Phys. Geogr.*, **31**, 455–472, doi:10.2747/0272-3646.31.5.455.
- Jury, M., B. A. Malmgren, and A. Winter, 2007: Subregional precipitation climate of the Caribbean and relationships with ENSO and NAO. *J. Geophys. Res.*, **112**, D16107, doi:10.1029/2006JD007541.
- Kalnay, E., and Coauthors, 1996: The NCEP/NCAR 40-Year Reanalysis Project. *Bull. Amer. Meteor. Soc.*, **77**, 437–471, doi:10.1175/1520-0477(1996)077<0437:TNYRP>2.0.CO;2.
- Karger, D. N., and Coauthors, 2016: Climatologies at High Resolution for the Earth's Land Surface Areas. 20 pp. [Available online at <https://arxiv.org/abs/1607.00217>]
- Karmalkar, A. V., R. S. Bradley, and H. F. Díaz, 2011: Climate change in Central America and Mexico: Regional climate model validation and climate change projections. *Climate Dyn.*, **37**, 605–629, doi:10.1007/s00382-011-1099-9.
- Karnauskas, K. B., J. P. Donnelly, and K. J. Anchukaitis, 2016: Future freshwater stress for island populations. *Nat. Climate Change*, **6**, 720–725, doi:10.1038/nclimate2987.
- Larsen, M. C., 2000: Analysis of 20th century rainfall and streamflow to characterize drought and water resources in Puerto Rico. *Phys. Geogr.*, **21**, 494–521.
- Leander, R., and T. A. Buishand, 2007: Resampling of regional climate model output for the simulation of extreme river flows. *J. Hydrol.*, **332**, 487–496, doi:10.1016/j.jhydrol.2006.08.006.
- Liu, W., and Coauthors, 2015: Extended Reconstructed Sea Surface Temperature version 4 (ERSST.v4): Part II. Parametric and structural uncertainty estimations. *J. Climate*, **28**, 931–951, doi:10.1175/JCLI-D-14-00007.1.
- Martin, E. R., and C. Schumacher, 2011: Modulation of Caribbean precipitation by the Madden-Julian oscillation. *J. Climate*, **24**, 813–824, doi:10.1175/2010JCLI3773.1.
- Maurer, E. P., and Coauthors, 2010: The utility of daily large-scale climate data in the assessment of climate change impacts on daily streamflow in California. *Hydrol. Earth Syst. Sci.*, **14**, 1125–1138, doi:10.5194/hess-14-1125-2010.
- McKee, T. B., N. J. Doesken, and J. Kleist, 1993: The relationship of drought frequency and duration to time scales. Preprints, *Eighth Conf. on Applied Climatology*. Anaheim, CA, Amer. Meteor. Soc., 179–184.
- Méndez, M., and V. Magaña, 2010: Regional aspects of prolonged meteorological droughts over Mexico and Central America. *J. Climate*, **23**, 1175–1188, doi:10.1175/2009JCLI3080.1.
- Monteith, J. L., 1965: Evaporation and environment. *19th Symp. of the Society for Experimental Biology*, Swansea, England, Society for Experimental Biology, 205–234.
- Mosier, T. M., D. F. Hill, and K. V. Sharp, 2014: 30-arcsecond monthly climate surfaces with global land coverage. *Int. J. Climatol.*, **34**, 2175–2188, doi:10.1002/joc.3829.
- Mueller, R., and Coauthors, 2013: Berkeley Earth temperature averaging process. *Geoinfo. Geostat. Overview*, **1** (2), doi:10.4172/2327-4581.1000103.
- OCHA, 2015: Drought in Central America in 2015: Situation report (as of October 6, 2015). United Nations Office for the Coordination of Humanitarian Affairs (OCHA). [Available online at http://www.redhum.org/uploads/documentos/pdf/Sitrep_OCHA-ROLAC_Drought_in_CA_EN_061015-20151006-AL-17144.pdf]
- Palmer, W. C., 1965: Meteorological drought. U.S. Weather Bureau Research Paper 45, 58 pp.
- Panofsky, H. A., and G. W. Brier, 1968: *Some Applications of Statistics to Meteorology*. Pennsylvania State University Press, 224 pp.
- Penman, H. L., 1948: Natural evaporation from open water, bare soil and grass. *Proc. Roy. Soc. London*, **193**, 120–145, doi:10.1098/rspa.1948.0037.
- Peters, E. J., 2015: The 2009/2010 Caribbean drought: A case study. *Disasters*, **39**, 738–761, doi:10.1111/disa.12123.
- Rauscher, S. A., and Coauthors, 2008: Extension and intensification of the Meso-American mid-summer drought in the twenty-first century. *Climate Dyn.*, **31**, 551–571, doi:10.1007/s00382-007-0359-1.
- Rohde, R., and Coauthors, 2013: A new estimate of the average Earth surface land temperature spanning 1753 to 2011. *Geoinfo. Geostat. Overview*, **1** (1), doi:10.4172/2327-4581.1000101.
- Roth, D. M., 2008: Hurricane Flora (1963) rainfall graphic. Tropical cyclone point maxima, National Weather Service. Accessed 9 June 2012. [Available online at <http://www.wpc.ncep.noaa.gov/tropical/rain/flora1963filledrainblk.gif>]
- Sahay, R., 2005: Stabilization, debt, and fiscal policy in the Caribbean. International Monetary Fund, Working Paper 05/26, 43 pp. [Available online at <https://www.imf.org/external/pubs/ft/wp/2005/wp0526.pdf>]
- Schneider, U., A. Becker, P. Finger, A. Meyer-Christoffer, B. Rudolf, and M. Ziese, 2015a: GPCC full data reanalysis version 7.0 at 1.0°: Monthly land-surface precipitation from rain-gauges built on GTS-based and historic data, doi:10.5676/DWD_GPCC/FD_M_V7_100.
- , —, —, —, and M. Ziese, 2015b: GPCC monitoring product: Near real-time monthly land-surface precipitation from rain-gauges based on SYNOP and CLIMAT data, doi:10.5676/DWD_GPCC/MP_M_V5_100.
- Schultz, D. M., W. E. Bracken, and L. F. Bosart, 1998: Planetary and synoptic-scale signatures associated with Central American cold surges. *Mon. Wea. Rev.*, **126**, 5–27, doi:10.1175/1520-0493(1998)126<0005:PASSA>2.0.CO;2.
- Sheffield, J., E. F. Wood, and M. L. Roderick, 2012: Little change in global drought over the past 60 years. *Nature*, **491**, 435–438, doi:10.1038/nature11575.

- Smerdon, J. E., B. I. Cook, E. R. Cook, and R. Seager, 2015: Bridging past and future climate across paleoclimatic reconstructions, observations, and models: A hydroclimate case study. *J. Climate*, **28**, 3212–3231, doi:[10.1175/JCLI-D-14-00417.1](https://doi.org/10.1175/JCLI-D-14-00417.1).
- Stephenson, T. S., and Coauthors, 2014: Changes in extreme temperature and precipitation in the Caribbean region, 1961–2010. *Int. J. Climatol.*, **34**, 2957–2971, doi:[10.1002/joc.3889](https://doi.org/10.1002/joc.3889).
- , and Coauthors, 2016: Regional climates: The Caribbean [in “State of the Climate in 2015”]. *Bull. Amer. Meteor. Soc.*, **97**, S181–S182, doi:[10.1175/2016BAMSStateoftheClimate.1](https://doi.org/10.1175/2016BAMSStateoftheClimate.1).
- Taylor, M. A., D. B. Enfield, and A. A. Chen, 2002: Influence of the tropical Atlantic versus the tropical Pacific on Caribbean rainfall. *J. Geophys. Res.*, **107**, 3127, doi:[10.1029/2001JC001097](https://doi.org/10.1029/2001JC001097).
- Thornthwaite, C. W., 1948: An approach toward a rational classification of climate. *Geogr. Rev.*, **38**, 55–94, doi:[10.2307/210739](https://doi.org/10.2307/210739).
- van der Schrier, G., P. D. Jones, and K. R. Briffa, 2011: The sensitivity of the PDSI to the Thornthwaite and Penman–Monteith parameterizations for potential evapotranspiration. *J. Geophys. Res.*, **116**, D03106, doi:[10.1029/2010JD015001](https://doi.org/10.1029/2010JD015001).
- , J. Barichivich, K. R. Briffa, and P. D. Jones, 2013: A scPDSI-based global data set of dry and wet spells for 1901–2009. *J. Geophys. Res. Atmos.*, **118**, 4025–4048, doi:[10.1002/jgrd.50355](https://doi.org/10.1002/jgrd.50355).
- Vicente-Serrano, S. M., S. Beguería, and J. I. López-Moreno, 2010: A multiscalar drought index sensitive to global warming: The standardized precipitation evapotranspiration index. *J. Climate*, **23**, 1696–1718, doi:[10.1175/2009JCLI2909.1](https://doi.org/10.1175/2009JCLI2909.1).
- Wells, N., S. Goddard, and M. J. Hayes, 2004: A self-calibrating Palmer drought severity index. *J. Climate*, **17**, 2335–2351, doi:[10.1175/1520-0442\(2004\)017<2335:ASPDSI>2.0.CO;2](https://doi.org/10.1175/1520-0442(2004)017<2335:ASPDSI>2.0.CO;2).
- Wilhite, D. A., M. D. Svoboda, and M. J. Hayes, 2007: Understanding the complex impacts of drought: A key to enhancing drought mitigation and preparedness. *Water Resour. Manage.*, **21**, 763–774, doi:[10.1007/s11269-006-9076-5](https://doi.org/10.1007/s11269-006-9076-5).
- Williams, A. P., R. Seager, J. T. Abatzoglou, B. I. Cook, J. E. Smerdon, and E. R. Cook, 2015: Contribution of anthropogenic warming to California drought during 2012–2014. *Geophys. Res. Lett.*, **42**, 6819–6828, doi:[10.1002/2015GL064924](https://doi.org/10.1002/2015GL064924).
- Wood, A. W., L. R. Leung, V. Sridhar, and D. P. Lettenmaier, 2004: Hydrologic implications of dynamical and statistical approaches to downscaling climate model outputs. *Climatic Change*, **62**, 189–216, doi:[10.1023/B:CLIM.0000013685.99609.9e](https://doi.org/10.1023/B:CLIM.0000013685.99609.9e).
- Zhao, T., and A. Dai, 2015: The magnitude and causes of global drought changes in the twenty-first century under a low-moderate emissions scenario. *J. Climate*, **28**, 4490–4512, doi:[10.1175/JCLI-D-14-00363.1](https://doi.org/10.1175/JCLI-D-14-00363.1).
- , and —, 2017: Uncertainties in historical changes and future projections of drought. Part II: Model-simulated historical and future drought changes. *Climatic Change*, doi:[10.1007/s10584-016-1742-x](https://doi.org/10.1007/s10584-016-1742-x), in press.